ACS APPLIED MATERIALS & INTERFACES

Research Article

www.acsami.org

Achieving Extremely Concentrated Aqueous Dispersions of Graphene Flakes and Catalytically Efficient Graphene-Metal Nanoparticle Hybrids with Flavin Mononucleotide as a High-Performance Stabilizer

M. Ayán-Varela,[†] J. I. Paredes,[†] L. Guardia,[†] S. Villar-Rodil,*[,†] J. M. Munuera,[†] M. Díaz-González,[‡] C. Fernández-Sánchez,[‡] A. Martínez-Alonso,[†] and J. M. D. Tascón[†]

[†]Instituto Nacional del Carbón, INCAR-CSIC, Apartado 73, 33080 Oviedo, Spain

[‡]Instituto de Microelectrónica de Barcelona, IMB-CNM (CSIC), Campus UAB, 08193 Bellaterra, Barcelona, Spain

Supporting Information

ABSTRACT: The stable dispersion of graphene flakes in an aqueous medium is highly desirable for the development of materials based on this two-dimensional carbon structure, but current production protocols that make use of a number of surfactants typically suffer from limitations regarding graphene concentration or the amount of surfactant required to colloidally stabilize the sheets. Here, we demonstrate that an innocuous and readily available derivative of vitamin B_2, namely the sodium salt of flavin mononucleotide (FMNS), is a highly efficient dispersant in the preparation of aqueous dispersions of defect-free, few-layer graphene flakes. Most notably, graphene concentrations in water as high as ~50 mg mL^{-1} using low amounts of FMNS (FMNS/graphene mass ratios of about 0.04) could be attained, which facilitated the formation of free-standing graphene films displaying high electrical conductivity (~52000 S m^{-1}) without the need of carrying out thermal annealing or other types of post-treatment. The excellent performance of FMNS as a graphene dispersant could be attributed to the combined effect of strong adsorption on the sheets through the isoalloxazine moiety of the molecule and efficient colloidal stabilization provided by its negatively charged phosphate group. The FMNS-stabilized graphene sheets could be decorated with nanoparticles of several noble metals (Ag, Pd, and Pt), and the resulting hybrids exhibited a high catalytic activity in the reduction of nitroarenes and electroreduction of oxygen. Overall, the present results should expedite the processing and implementation of graphene in, e.g., conductive inks, composites, and hybrid materials with practical utility in a wide range of applications.

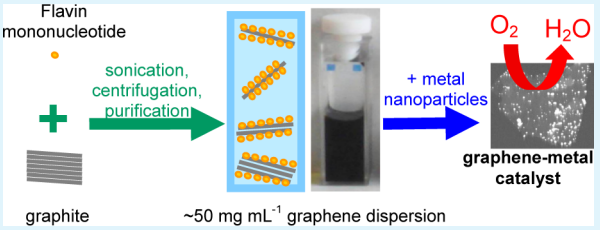

KEYWORDS: *graphene, graphene dispersions, biodispersants, graphene-nanoparticle hybrids, catalytic reduction*

1. INTRODUCTION

As a two-dimensional carbon material with outstanding physical properties and a strong potential for application in many relevant technological areas (e.g., electronics, photonics, energy conversion and storage, chemical sensing and biosensing, catalysis, or biomedicine), graphene is currently the focus of intense research efforts worldwide.[1−3] To fulfill the prospect of using graphene in large-scale industrial applications, simple and inexpensive methods for its mass production with controlled characteristics must be developed, and consequently, over the past few years a great deal of research has been directed toward achieving this goal.[3,4] So far, a number of both bottom-up and top-down approaches for the preparation of different types of graphene have become available. Among the former, chemical vapor deposition of hydrocarbons onto suitable substrates (typically metals, such as copper) is particularly attractive, as it affords large-area, mostly defect-free graphene films suitable for high-end applications in, e.g, electronics or photonics.[3−6] However, in many other instances having large numbers of graphene sheets in the form of colloidal dispersions or inks would be preferable, and in such cases top-down methods based on the exfoliation of graphite and graphite derivatives appear as a viable technological option.[3,4,7,8]

Although the exfoliation and subsequent reduction of graphite oxide has been extensively investigated as a convenient means of affording bulk quantities of graphene-like sheets (reduced graphene oxide sheets) with practical utility in many areas,[9−13] the resulting material generally contains a significant amount of residual oxygen and structural imperfections and is thus of limited interest when pristine, defect-free graphene sheets are sought after.[14,15] In the latter case, direct exfoliation of graphite in the liquid phase, usually triggered by ultrasound waves, has been proposed as a simple and efficient alternative.[16−18] Indeed, early work by Coleman et al.

Received: January 30, 2015
Accepted: April 27, 2015
Published: April 27, 2015

DOI: 10.1021/acsami.5b00910
ACS Appl. Mater. Interfaces 2015, 7, 10293−10307

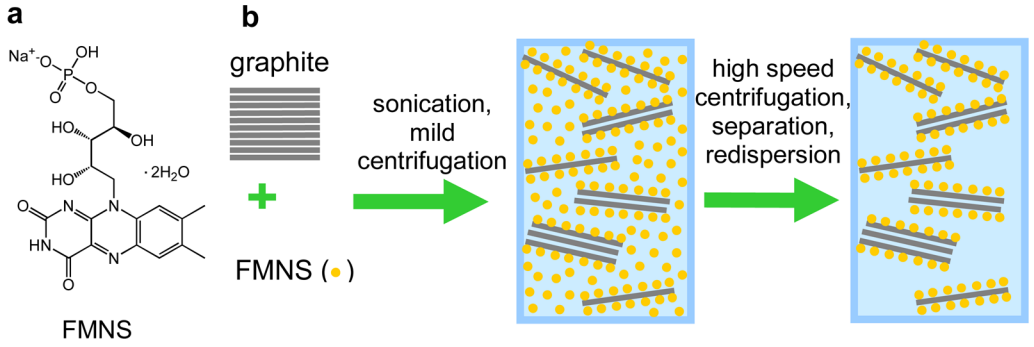

Figure 1. (a) Chemical structure of the sodium salt of flavin mononucleotide. (b) Schematic illustrating the preparation and purification of colloidal dispersions of graphene stabilized by FMNS.

demonstrated that pristine graphite can be exfoliated and dispersed in solvents with surface energy matching or close to that of the basal plane of graphite (~70 mJ m^{-2}), yielding stable colloidal dispersions of single- to few-layer graphene sheets.[19] Suitable solvents for dispersing graphene include *N*,*N*-dimethylformamide, *N*-methyl-2-pyrrolidone, or cyclopentanone.[20] These are generally high boiling point and non-innocuous solvents, which pose concerns regarding their manipulation and processing in the fabrication of graphene-based materials and devices. Thus, from both an environmental and a practical perspective, working with graphene dispersions in water would be clearly advantageous, but its high surface energy implies that graphene sheets cannot be stably dispersed in water alone. An exception in this regard has been very recently reported with the preparation of stable dispersions of multilayer graphene in a weakly basic aqueous medium, but only very low graphene concentrations (<0.02 mg mL^{-1}) could be attained with this approach.[21] Nevertheless, to overcome this limitation, appropriate surfactants or stabilizers can be employed.[16−18]

Over the past few years, a number of dispersants have been used toward the exfoliation and stabilization of graphite to yield aqueous suspensions of graphene sheets. These include ionic surfactants (sodium dodecylbenzenesulfonate, sodium cholate, etc.),[22−27] nonionic/polymeric surfactants (e.g., polyvinylpyrrolidone and Pluronic copolymers),[24,26,28−33] and dye or fluorescent molecules consisting of a planar polyaromatic core (usually pyrene) decorated with pendant ionic/hydrophilic groups[34−39] as well as large biomolecules (e.g., RNA and some proteins and enzymes).[40−45] The resulting aqueous dispersions have facilitated the incorporation of graphene in different systems with practical utility, for example, transparent conductors,[23,41] supported catalysts,[25,44] solar cells,[26] gas sensors,[35] supercapacitors,[32,35] or polymer composites.[36] Nevertheless, to take full advantage of this colloidal approach as a convenient means to access pristine graphene sheets in bulk quantities suitable for the broadest possible range of applications, the dispersants should satisfy several requirements that most of the stabilizers employed previously to this end do not fully meet. First, to expedite the production and processing of the aqueous suspensions, the dispersant should afford very high concentrations of colloidally stabilized graphene sheets. Second, because the dispersant is usually difficult to remove and its presence can be detrimental to the performance of materials and devices obtained from the aqueous suspensions, the amount of dispersant required to stabilize a given amount of graphene should be as low as possible. State-of-the-art aqueous graphene dispersions typically attain concentrations of a few to several milligrams per milliliter using commensurate amounts of stabilizer (stabilizer/graphene mass ratios above ~0.4).[25,31,39] Achieving larger graphene concentrations with significantly lower amounts of dispersant would be clearly advantageous. Third, for safety and environmental reasons, the dispersant molecules should be innocuous and nontoxic. In this regard, the use of benign and readily available biomolecules would be an undoubtedly attractive feature, but the different biomolecules tested so far have not demonstrated significantly high graphene concentrations. Therefore, the identification of high-performing, safe (bio)dispersants for the stabilization of aqueous graphene dispersions is in great demand.

Here, we report the sodium salt of flavin mononucleotide (FMNS) to be one such high-performing biodispersant for graphene flakes. FMNS (riboflavin-5′-phosphate sodium salt) is an essentially innocuous derivative of riboflavin (vitamin B_2) that is involved in metabolic processes occurring in living cells and is also employed as a food additive.[46] Although flavin mononucleotide has very recently been put forward as a successful surfactant for graphene nanosheets[47] and previously for carbon nanotubes,[48,49] here we show for the first time that it is a truly exceptional surfactant in that it can stabilize very high concentrations of graphene sheets in an aqueous medium (up to ~50 mg mL^{-1}) using very low biomolecule/graphene mass ratios (~0.04). To the best of our knowledge, such performance has not been previously reported for aqueous graphene dispersion with any (bio)surfactant. Our findings suggest that FMNS could be used as a key component in the development of high-throughput approaches toward graphene colloidal dispersions and inks. Furthermore, we demonstrate the potential utility of the FMNS-stabilized graphene suspensions by synthesizing graphene-noble metal (Ag, Pt, Pd) nanoparticle (NP) hybrids, which exhibit a high catalytic activity in the reduction of nitroarenes and good performance as electrocatalysts toward the oxygen reduction reaction, with a possible use in electrochemical oxygen sensing.

2. RESULTS AND DISCUSSION

2.1. Preparation and Characterization of FMNS-Stabilized Aqueous Graphene Dispersions. Figure 1a shows the chemical structure of FMNS. FMNS is an amphiphilic molecule that consists of a tricyclic heteronuclear organic ring (dimethylated isoalloxazine) appended with a phosphorylated alcohol (ribitol) moiety[46,50] Such a structure endows FMNS with some features that are central for its use as an efficient stabilizer of graphene sheets in an aqueous medium. More specifically, due to its planar, hydrophobic, and partially aromatic character, the isoalloxazine component of FMNS can

DOI: 10.1021/acsami.5b00910
ACS Appl. Mater. Interfaces 2015, 7, 10293−10307

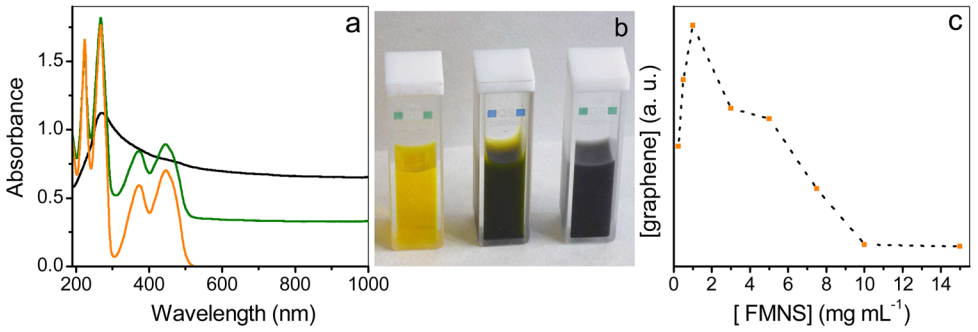

Figure 2. (a) UV−vis absorption spectrum of FMNS aqueous solution (orange trace), aqueous graphene dispersion stabilized with 1 mg mL^{-1} FMNS before (green trace) and after purification (black trace). (b) Digital photograph of the dispersions in a after dilution to avoid saturation of the signal. From left to right: 1 mg mL^{-1} FMNS aqueous solution, 0.3 mg mL^{-1} aqueous graphene dispersion stabilized with 1 mg mL^{-1} FMNS before and after purification. The dilution used is 1:40 in the first case and 1:10 in the other two. (c) Concentration of dispersed graphene as a function of FMNS concentration.

be expected to strongly adsorb onto the basal plane of graphite/graphene. In addition, the polar, hydrophilic phosphorylated alcohol moiety of the molecule will extend into the aqueous phase, thus providing colloidal stability to graphene sheets via electrostatic repulsion between negatively charged phosphate groups. As a matter of fact, bath sonication of graphite powder in aqueous FMNS solutions followed by mild centrifugation of the resulting dispersions afforded black-colored supernatants that were indicative of the successful exfoliation and colloidal stabilization of the graphite particles. The resulting dispersions were further processed by repeated cycles of sedimentation through high-speed centrifugation and resuspension in pure water to get rid of as many free, nonadsorbed FMNS molecules as possible, finally yielding stable graphene suspensions with minimized FMNS/graphene mass ratios (see Figure 1b for a schematic of the preparation procedure). Alternatively, the free FMNS fraction could be removed by dialysis. Indeed, the dispersions could be dialyzed for long periods of time (e.g., weeks) without showing any visible sign of agglomeration or precipitation, this being a first indication that the exfoliated graphite particles had been colloidally stabilized by a small amount of strongly adsorbed FMNS molecules. Actually, FMNS was selected as the best candidate for the stabilization of graphene in colloidal solution from a bench of different natural compounds containing an aromatic functionality along with phosphate groups, such as vitamin B_6 phosphate, on the basis of a previous survey study on their performance. Riboflavin alone (i.e., FMNS without the phosphate group) adsorbed onto the graphene surface but was not effective in colloidally stabilizing the flakes.

Figure 2a (orange plot) shows the typical UV−vis absorption spectrum of FMNS in aqueous solution, which is dominated by strong absorption bands in the 200−500 nm wavelength range, null absorption being recorded at higher wavelengths.[46,51] As noticed in the digital photograph of Figure 2b (left cuvette), aqueous FMNS solutions exhibit a distinctive yellow color. The presence of such bands was still apparent in the FMNS-stabilized graphene dispersions before carrying out the sedimentation-resuspension cycles that were intended to remove the free FMNS molecules (cuvette in the middle of Figure 2b and green plot in Figure 2a). However, in this case, significant absorbance was seen in the whole wavelength range above 500 nm, consistent with the presence of graphitic material in the dispersion.[24] By contrast, after purification of the dispersions via the iterative sedimentation-resuspension process, the absorption bands characteristic of FMNS vanished almost completely, and the recorded spectrum was that archetypal of pristine graphene sheets (black plot in Figure 2a). More to the point, a single band at ∼272 nm was observed, which could be attributed to $\pi \rightarrow \pi^*$ transitions in extended electronically conjugated carbon structures, together with strong absorbance in the visible and near-infrared range.[24,25,29] The latter feature led to the well-known opaque black tone characteristic of dispersions of graphenic materials, including pristine graphene and reduced graphene oxide (Figure 2b, right cuvette).[24,31,52,53] These results suggest that the iterative purification process is remarkably efficient in eliminating the free FMNS fraction from the aqueous dispersions and that just a relatively small amount of this amphiphile (compared with the amount of suspended graphitic material) is actually required to stabilize the exfoliated sheets. This is an important point that is usually not considered in the litereature concerning the colloidal stabilization of graphene with surfactants. Indeed, the purified dispersions were seen to be stable for at least six months, standing visually homogeneous throughout without showing significant precipitation. Hence, we assume that only a relatively small amount of FMNS molecules remain in the dispersion, and they are for the most part strongly adsorbed on the exfoliated sheets, providing them with a high colloidal stability in the aqueous medium. Below, we will present further indication that this is indeed the case.

We then sought to optimize the preparation procedure of these suspensions (mainly in terms of the amount of material that could be exfoliated and dispersed) by investigating the influence of several experimental parameters, such as the initial concentration of graphite powder and FMNS, sonication time, or centrifugation conditions. For graphite powder with the typical particle sizes used here (∼2−20 μm), control experiments revealed a starting graphite concentration of 30 mg mL^{-1} to be reasonable for the exfoliation of this material. Lower initial graphite concentrations yielded correspondingly lower concentrations of exfoliated sheets in the aqueous medium, while significantly higher starting concentrations did not result in equally higher concentrations of the exfoliated phase. Similar observations have been recently reported in the exfoliation of graphite and other layered materials in water using different stabilizers.[33,54] Although the origin of the reduced exfoliation efficiency at the higher initial graphite concentrations is currently not understood, it could be possibly related to changes in the generation and/or collapse of cavitation bubbles,

DOI: 10.1021/acsami.5b00910
ACS Appl. Mater. Interfaces 2015, 7, 10293−10307

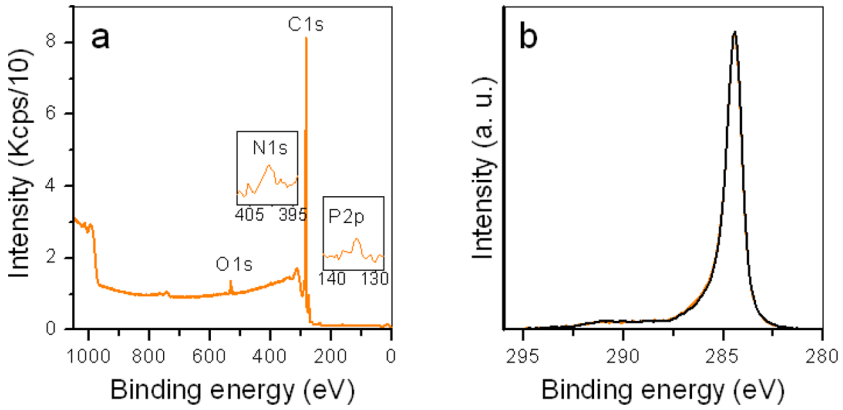

Figure 3. XPS spectra of the dried 0.3 g mL^{-1} aqueous graphene dispersion stabilized with FMNS. (a) XPS survey spectrum with insets where the intensity has been magnified for the binding energy range of N 1s and P 2p core levels. (b) Background-corrected, normalized, high resolution C 1s core level XPS spectrum of the graphene dispersion stabilized with FMNS (orange line) and the bulk, starting graphite (black line).

which are thought to be responsible for the delamination of the material, as a result of the presence of large fractions of solid particles in the liquid medium.[54,55]

As shown in Figure 2c, the amount of graphite that could be exfoliated and stably suspended in the aqueous medium was also seen to be highly sensitive to the initial concentration of FMNS. Such an amount first increased steeply and then steadily decreased with increasing FMNS concentration, reaching a maximum at about 1 mg mL^{-1} of the amphiphile. At high initial FMNS concentrations (i.e., 10 mg mL^{-1} and above), very little graphitic material could be dispersed. Again, this type of behavior, where the amount of dispersed material goes through a maximum value with increasing concentration of stabilizer, has been documented beforehand for a number of layered materials and surfactant–water systems, and different explanations have been proposed to account for it.[22,25,36,39,54] In the case of some stabilizers with a planar, aromatic core that strongly adsorbs onto the graphene surface and an ionizable moiety that provides colloidal stability to the graphene sheets through electrostatic repulsion, the dissociation degree of the ionizable group has been shown to decrease above a given concentration, thus leading to a reduction in the colloidal stability, and consequently in the concentration, of aqueous graphene dispersions.[36,39] In the particular instance of FMNS, because its negatively charged phosphate group lies relatively far apart from its planar, hydrophobic core, there is also the possibility that it undergoes self-association via $\pi-\pi$ or hydrophobic interactions at higher concentrations in water. Indeed, it has been shown that this amphiphile possesses a strong propensity to form dimers (but not higher-order structures) in aqueous solution, with the molar fraction of molecules participating in dimeric structures increasing notably as the FMNS concentration is increased.[56] As a result of this competitive self-association process, the thermodynamic drive for adsorption of FMNS on the graphene surface can be expected to diminish, so that the exfoliated sheets would become less efficiently stabilized in the aqueous medium at increasing concentrations of the amphiphilic molecule. We stress that the origin of the observed FMNS concentration dependence is not completely clear and its elucidation will most probably require in-depth studies, which are beyond the scope of the present work. In any case, we do not believe that such behavior is related to any chemical modification of the FMNS molecules during the preparation of the graphene dispersions. For example, sonication of aqueous FMNS solutions, which could be the most obvious source of chemical modification, did not give rise to any significant change in the four characteristic UV–vis absorption bands of the molecule.

Optimization of sonication time and centrifugation speed was also carried out. Consistent with previous reports on the exfoliation of graphite in aqueous surfactant solutions to give graphene sheets,[24] the amount of dispersed graphitic material increased steadily with sonication time up to about 5 h, with longer ultrasound treatments failing to provide significantly higher concentrations of exfoliated sheets. The centrifugation speed was adjusted to a value of 1500–2300 rpm (20 min) so as to afford sedimentation of unexfoliated graphite particles/thicker exfoliated sheets and to maximize at the same time the concentration of dispersed material that was colloidally stable for at least a few months, showing little or no sign of precipitation to the naked eye. We note that, during the subsequent iterative purification process implemented to remove the free, nonadsorbed FMNS fraction from the obtained dispersions, sedimentation of the exfoliated sheets was accomplished at 14 600 rpm (20 min). The optimized preparation procedure (initial graphite powder and FMNS concentrations of 30 and 1 mg mL^{-1}, respectively; sonication for 5 h; centrifugation at 2300 rpm for 20 min) typically afforded dispersed concentrations (both before and after the purification step) of about 0.3 mg mL^{-1}, implying exfoliation yields (~1%) that are comparable to, or even better than, those reported for other efficient dispersants of graphene sheets.[22,24,25,28,29,33,36,39]

The miscrocopic characterization by transmission electron microscopy (TEM) and atomic force microscopy (AFM) showed that the suspension consisted typically of flakes with lateral dimensions of a few hundreds of nanometers and five or less monolayers thick (see Supporting Information for details). Raman spectroscopy provided evidence that the exfoliated flakes were of a high structural quality (see Supporting Information for details). Only carbon, oxygen, nitrogen, and phosphorus were detected in the X-ray photoelectron spectroscopy (XPS) survey spectra of the dry graphene powder (Figure 3a). The percentage of phosphorus was very low (~0.1) but nonetheless above the detection limit of this technique. The presence of phosphorus could only be due to the phosphate group of the FMNS molecule, because neither the starting graphite nor the material exfoliated in a phosphorus-free medium (e.g., in water–isopropanol mixtures without surfactant)[57] exhibited any detectable signal for this

DOI: 10.1021/acsami.5b00910
ACS Appl. Mater. Interfaces 2015, 7, 10293–10307

element by XPS. Consequently, the amount of phosphorus determined by XPS can be used to estimate the molar and mass ratios of FMNS to graphene in the purified dispersions, which were about 1×10^{-3} and 0.04, respectively. This FMNS/graphene mass ratio is at least 1 order of magnitude lower than the values that have been generally used in the stabilization of aqueous graphene suspensions with efficient surfactants,[24,25,29,31,36,39] thereby highlighting the exceptional performance of FMNS as a graphene dispersant. The marginal amount of FMNS was also suggested by the fact that no apparent indication of bands that could be associated with specific molecular groups of FMNS were detected by attenuated total reflection Fourier transform infrared (ATR-FTIR) spectroscopy (see Supporting Information for details). The XPS data also indicated that the nitrogen present in our graphene samples came exclusively from FMNS, since the measured nitrogen/phosphorus atomic ratio (4:1) equaled that of its molecular formula. However, the same did not hold true in the case of oxygen: the oxygen/phosphorus atomic ratio derived by XPS was 22:1, compared with a ratio of 9:1 for the FMNS molecule. We do not believe that this amount of extra oxygen in the graphene samples is related to oxidation of the exfoliated sheets. Indeed, their high resolution C 1s core level spectrum (Figure 3b, orange plot) was virtually identical to that of the starting, pristine graphite sample (black plot), implying that the graphene sheets in the FMNS-stabilized dispersions had not been oxidized to any significant extent. We hypothesize that the extra oxygen arises from water molecules strongly adsorbed around the hydrophilic segment of the FMNS amphiphile.

The FMNS-stabilized aqueous graphene dispersions could be readily processed into thin, free-standing paper-like films by vacuum filtration, and their electrical conductivity was measured by the van der Pauw method, yielding typical values of about 52 000 S m^{-1}. To the best of our knowledge, these are the highest conductivity values (by a factor of at least 5) that have been reported for as-prepared, graphene films obtained from their corresponding surfactant-stabilized dispersions in water. Table 1 compares conductivity values collected from the literature for a number of films prepared from suspensions of essentially defect-free graphene flakes in different surfactant−water solutions or organic solvents.[22−25,39,43,58−63] For graphene films derived from aqueous surfactant-based suspensions, relatively high conductivities (>10 000 S m^{-1}) have been only typically attained following a thermal annealing step at moderate temperatures, which was not required in our case. Anyhow, as noticed from Table 1, conductivity values similar or even higher than those of our FMNS-based films have been only accomplished with annealed films prepared from organic solvent dispersions. The remarkable performance of the FMNS-based graphene films described here can be attributed to both the high structural quality of the exfoliated sheets and, probably more importantly, to the low mass fraction of FMNS present in the films, the latter implying that electrical contacts between neighboring sheets will not be severely hampered as is the case for films incorporating large fractions of surfactant.[22,24] Indeed, in a very recent report, the sheet resistance of graphene films prepared from (non-purified) dispersions stabilized with flavin mononucleotide before and after annealing was 1800 and 130 Ω sq^{-1},[47] respectively, while the corresponding sheet resistance of our films is ∼0.5 Ω sq^{-1}. In that report, the flavin to graphene mass ratio of the dispersion was about 83.[47]

Table 1. Comparison of Electrical Conductivity Values for Different Oxygen-Free, Low-Defect Content Graphenes Obtained through Exfoliation (Mostly, although Not Exclusively, Based on Sonication) and Subsequent Colloidal Stabilization of Graphite Either in Water Assisted by Surfactants or in Other Solvents[a]

method of graphite exfoliation and stabilization	electrical conductivity (S m^{-1})	ref
sonication in water with sodium docecylbenzenesulfonate	35	22
	1500 (250 °C, Ar/N_2)	
sonication in water with sodium cholate	2000	23
	15 000 (500 °C, H_2/Ar)	
sonication in water with poly(sodium 4-styrenesulfonate)	3600	24
sonication in water with sodium taurodeoxycholate	13 000 (600 °C, H_2/Ar)	25
sonication in water with naphthalene diimide-based surfactants	4717	39
sonication in water with gum Arabic (GA)	10 000 (after GA removal by acid hydrolysis)	43
high-shear mixing in NMP	20 000	58
	40 000 (250 °C, H_2/Ar)	
sonication in NMP	18 000	59
sonication in *o*-dichlorobenzene	1500 (400 °C, vacuum)	60
electrochemical exfoliation in aqueous solution of inorganic salt and dispersion in DMF	8270	61
	22 250 (300 °C, H_2/Ar)	
intercalation of eutectic salt and dispersion in pyridine	5400	62
	91 000 (300 °C, H_2)	
spontaneous exfoliation and dispersion in chlorosulfonic acid	110 000	63
sonication in water with FMNS	52 000	present work

[a]In some cases, conductivity values are also given for the same films after heat treatment, the temperature and annealing atmosphere of which are indicated in parentheses.

Even though the purified graphene dispersions contained a low amount of FMNS, the presence of this molecule strongly adsorbed on the exfoliated sheets could be easily detected by means of cyclic voltammetry (CV). Figure 4a (orange traces) shows CVs recorded for thin FMNS-stabilized graphene films deposited onto a GCE in deoxygenated 0.1 M phosphate buffer saline (PBS) at pH 7.4 and scan rate of 50 mV s^{-1} in the potential region between 0 and −0.9 V vs Ag/AgCl. These CVs exhibited one anodic and one cathodic peak that were not present for GCE-supported graphene films obtained from exfoliated graphite in water−isopropanol mixtures in the absence of FMNS or any other stabilizer (black trace in Figure 4a).[57] The intensity of these peaks increased with the increasing amount of FMNS-stabilized graphene deposited onto the GCE [(total mass of deposited graphene: 0.3 μg (dashed orange trace), 1.2 μg (solid orange trace)], and their half-wave potential (−0.5 V vs Ag/AgCl) could be related to oxidation/reduction processes of FMNS[64] (see Supporting Information for further demonstration of the origin of these peaks being due to the FMNS molecules).

Figure 4b presents CVs for FMNS-stabilized graphene films (1.2 μg) recorded at different scan rates. Both anodic and cathodic currents were seen to increase linearly with this parameter (inset to Figure 4b), revealing that the electrode

DOI: 10.1021/acsami.5b00910
ACS Appl. Mater. Interfaces 2015, 7, 10293−10307

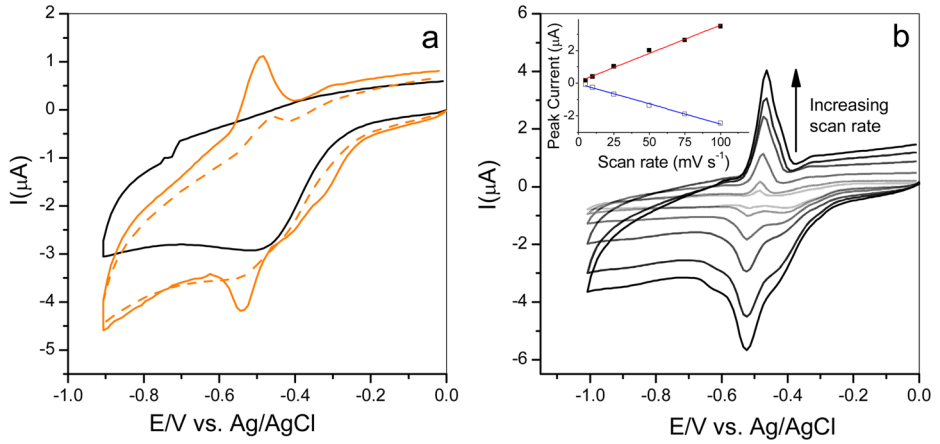

Figure 4. (a) Cyclic voltammogramas obtained in PBS at pH 7.4 with GCEs modified with 1.2 μg of graphene (black line), 0.3 μg graphene-FMNS (orange, dashed line), and 1.2 μg graphene-FMNS (orange, solid line). Scan rate: 50 mV/s. (b) Cyclic voltammogramas obtained in PBS at pH 7.4 with GCEs modified with 1.2 μg of graphene-FMNS at different scan rates: 5, 10, 25, 50, 75, and 100 mV s^{-1}, shown in lines in increasing tone from light gray to black. The inset shows the values of the anodic (filled squares) and cathodic (empty squares) peak currents. Their linear dependence with the scan rate is represented in red and blue solid lines, respectively.

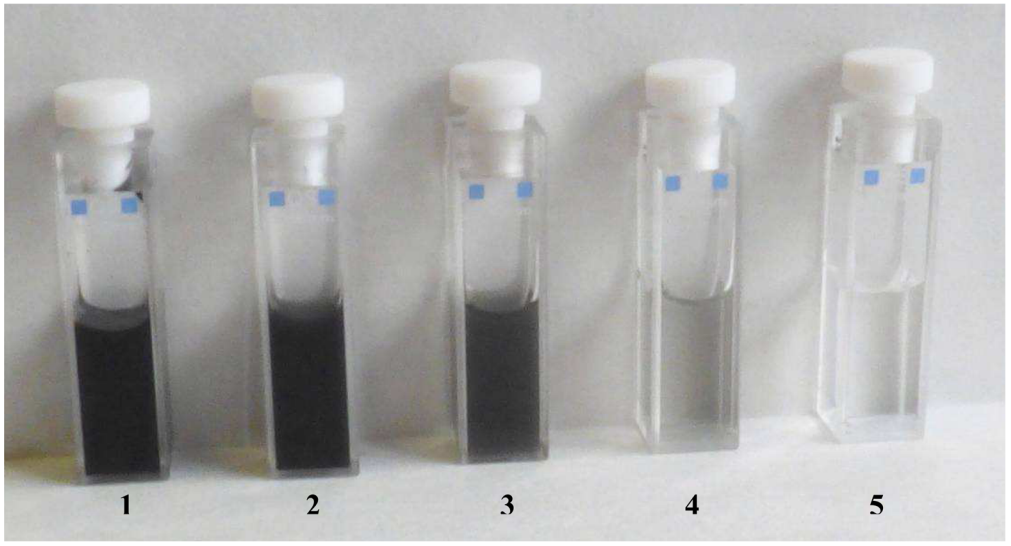

Figure 5. Digital photograph of as prepared 45 mg mL^{-1} graphene dispersion stabilized with FMNS (cuvette 1), the same dispersion diluted by a factor of 100 (2), 1000 (3), 5000 (4), and pure milli-Q water (5).

process was controlled by adsorption. Indication of strong adsorption of the FMNS molecules on the graphene sheets was obtained by continuous potential cycling between 0 and −0.9 V vs Ag/AgCl at 100 mV s^{-1}: up to 20 cycles were sequentially recorded, and all of them were virtually identical to each other, proving the high stability of the FMNS-based electrode. This result clearly points to the idea that the sedimentation-resuspension protocol used here to purify the graphene dispersions was very effective in removing the free FMNS fraction, and that the FMNS molecules remaining in the graphene suspension were firmly attached to the exfoliated sheets, thereby stabilizing them in the aqueous medium.

We have demonstrated that FMNS is able to colloidally stabilize the sheets at low mass ratios (~0.04 relative to graphene), which is an important feature when considering practical applications of the FMNS-based suspensions. However, similar to what has been very recently reported in the literature,[47] the concentration of graphene in the as-prepared dispersions was relatively low (~0.3 mg mL^{-1}), whereas much higher values would be required for such dispersions to be of truly practical utility, for instance in the development of high performance, conductive graphene-based inks. We believe that this low graphene concentration is mostly related to the low exfoliation yield that is usually associated with the use of ultrasound[7,17,18,22] rather than to the suspending ability of FMNS having reached its limit. Indeed, significantly higher graphene concentrations (a few to several milligrams per milliliter) could be easily achieved by using graphite powder that had been pre-exfoliated by sonication in water-isopropanol mixtures. In the pursuit of even higher concentrations, two additional protocols were explored. In one of them, the purified dispersions were concentrated up to 30−40 mg mL^{-1} by removal of water in a rotary evaporator. In the second protocol, the dispersions were subjected to iterative steps of sedimentation by centrifugation and resuspension in an aqueous FMNS solution (1 mg mL^{-1}) of half the initial dispersion volume, thus doubling the graphene concentration after each sedimentation-resuspension step. This procedure

DOI: 10.1021/acsami.5b00910
ACS Appl. Mater. Interfaces 2015, 7, 10293−10307

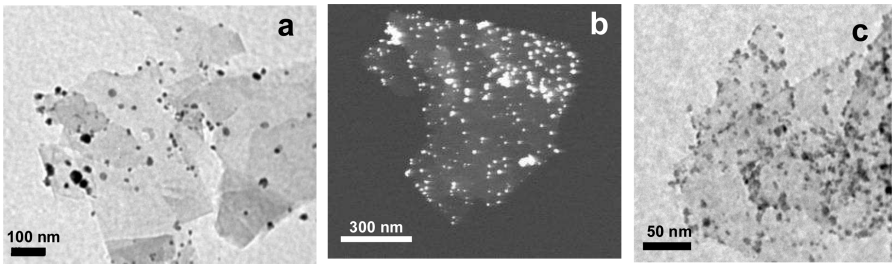

Figure 6. Microscopic characterization of the graphene–metal NP hybrids: (a) bright-field TEM image of the graphene–Ag NP hybrid, (b) dark-field STEM image of graphene–Pd NP hybrid prepared by reduction with ethanol, and (c) bright-field TEM image of the graphene–Pt NP hybrid.

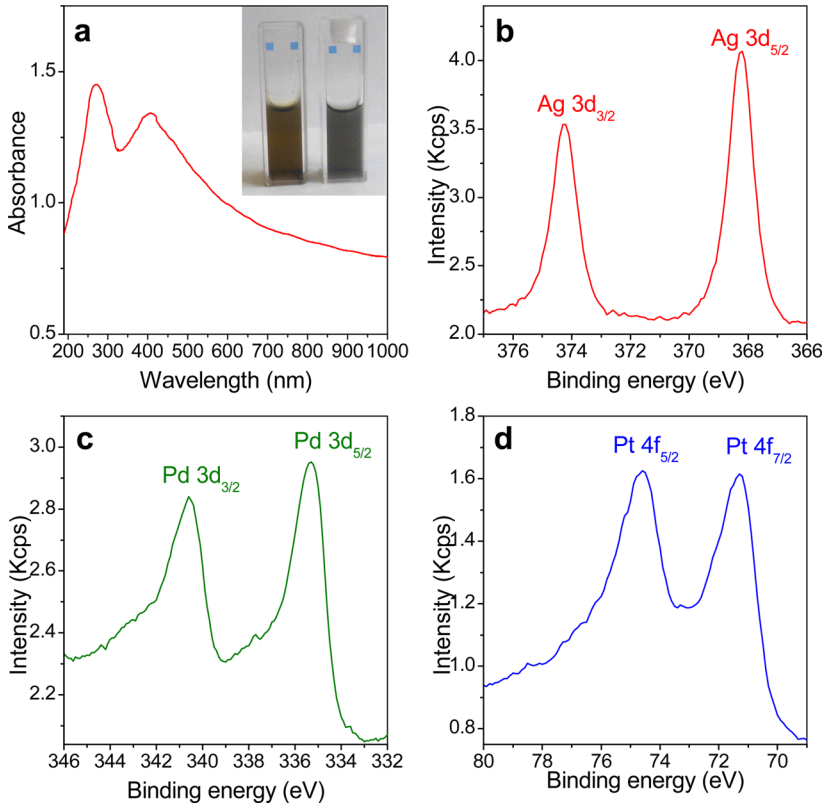

Figure 7. Spectroscopic characterization of graphene–metal NP hybrids. (a) UV–vis absorption spectrum of the graphene–Ag NP hybrid. In the inset, digital photograph of graphene dispersion (right) and graphene–Ag NP hybrid (left). High resolution XPS spectrum of (b) Ag 3d, (c) Pd 3d, (d) Pt 4f for the graphene–Ag, Pd, and Pt NP hybrids, respectively.

afforded graphene concentrations as high as ~50 mg mL^{-1}, which are to the best of our knowledge the highest reported to date for pristine graphene sheets in aqueous medium. Furthermore, the fraction of FMNS required for such high concentration (~0.04) is very much below the previous value reported in the literature for much lower graphene concentration (flavin mononucleotide to graphene mass ratio of ~83 for graphene concentrations of 0.24 mg mL^{-1}).[47] Figure 5 (cuvette 1) shows a digital photograph of such highly concentrated dispersion, together with the same dispersion after dilution in water by a factor of 100 (2), 1000 (3), and 5000 (4), as well as a cuvette containing only water for comparison (5). These highly concentrated dispersions were quite stable, showing only a very little amount of precipitate after being stored for several days.

2.2. Synthesis of Metal NPs on FMNS-Stabilized Graphene Sheets and Investigation of the Catalytic and Electrocatalytic Performance of the Resulting Hybrids.

Due to its high surface area, superior electrical and thermal conductivity, as well as good mechanical and chemical stability, graphene is considered an ideal support of metal and semiconducting NPs with a strong potential toward different catalytic, electrocatalytic, and photocatalytic applications.[65−67] While most of the studies in this context are focused on chemically modified forms of graphene, most notably graphene oxide (GO) and reduced graphene oxide (RGO), the use of pristine graphene sheets as NP support has been comparatively uncommon. This can be put down to the fact that, in contrast to the abundant oxygen functional groups that typically decorate GO/RGO sheets and serve as anchoring sites for the nucleation and growth of NPs, the rather inert and unreactive nature of the basal plane of pristine graphene does not generally favor the firm attachment of NPs. In our case, however, it can be anticipated that the presence of phosphate groups on the sheet surface will promote the anchoring of NPs on the FMNS-stabilized graphene. Compared to the case of

DOI: 10.1021/acsami.5b00910
ACS Appl. Mater. Interfaces 2015, 7, 10293−10307

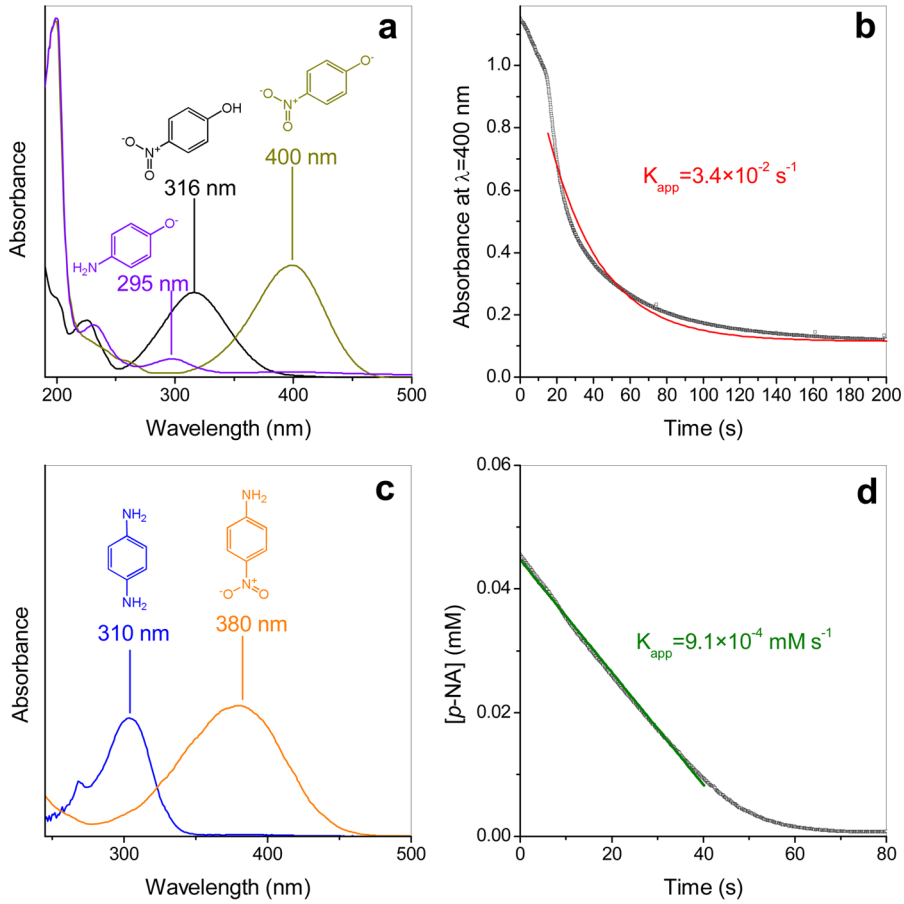

Figure 8. (a) UV−vis absorption spectra of *p*-NP (black curve), *p*-nitrophenoxide ion (dark yellow), and *p*-aminophenoxide ion (violet). The absorption peak at 400 nm of *p*-nitrophenoxide is used to monitor its conversion to *p*-aminophenoxide by reduction with $NaBH_4$. (b) Plot of absorbance at 400 nm for the reduction of 4-nitrophenoxide with $NaBH_4$ as catalyzed by graphene−Pd NP hybrids stabilized in the aqueous dispersion by FMNS. The experimental kinetic profile could be fitted to an exponential decay function, which is shown as an overlaid red line. The corresponding apparent rate constant (k_{app}) is also shown. Experimental conditions: [*p*-NP] = 0.06 mM; [$NaBH_4$] = 36 mM; [Pd] = 0.5 μg mL^{-1}. (c) UV−vis absorption spectra of *p*-NA (green trace) and *p*-PDA (blue). The absorption peak at 380 nm of *p*-NA is used to monitor the reaction progress. (d) Plot of absorbance at 380 nm for the reduction of *p*-NA with $NaBH_4$ as catalyzed by graphene−Ag NP hybrids stabilized in the aqueous dispersion by FMNS. The experimental kinetic profiles could be fitted to a straight line which is shown as an overlaid green line. The corresponding apparent rate constant (k_{app}) is also shown. Experimental conditions: [*p*-NA] = 0.06 mM; [$NaBH_4$] = 36 mM; [Ag] = 0.7 μg mL^{-1}.

GO, this approach has the advantage that the graphene sheets are obtained by a very simple procedure, avoiding the harsh oxidation protocols typically required for the preparation of GO. Indeed, we were able to grow Ag, Pd, and Pt NPs selectively on the FMNS-stabilized graphene sheets by reduction of the corresponding metal salts following the wet chemical methods described in the Experimental Section. Evidence for the decoration of the sheets with the metal NPs was obtained from TEM/ scanning transmission electron microscopy (STEM) imaging, UV−vis absorption spectroscopy (only for Ag), and XPS. Figure 6 shows some representative images of the different graphene−metal NP hybrids (Ag NPs, a; Pd NPs prepared via reduction with ethanol, b; Pt NPs, c). In general, the NPs could be grown exclusively on the FMNS-stabilized sheets (no stand-alone NPs were seen in the images) and tended to uniformly decorate the sheets. Typical NP sizes were about 15−25 nm (Ag), 5−10 nm (Pd prepared via reduction with $NaBH_4$), 10−15 nm (Pd prepared via reduction with ethanol), and 3−6 nm (Pt).

A typical UV−vis absorption spectrum of the graphene−Ag NP hybrid is presented in Figure 7a. In addition to the absorption band located at about 272 nm, arising from the graphene sheets (see above), there is a strong peak at ∼410 nm that can be ascribed to the surface plasmon resonance (SPR) band characteristic of metallic silver nanostructures.[68] Indeed, the presence of the latter was visually evident from the yellowish tone of the aqueous dispersions of this hybrid, which is in contrast to the grayish color of dispersions that only contain graphene sheets at the same concentration (see inset to Figure 7a). Neither Pd- nor Pt-based metallic nanostructures displayed optical absorption bands, but evidence for the presence of these two elements, as well as Ag, in metallic form in the hybrids could be gathered by XPS.

Figure 7b−d shows high resolution core level spectra for Ag 3d (b), Pd 3d (c), and Pt 4f (d) from the different hybrid samples. In each case, a doublet band could be noticed, which appeared at binding energies typical of the corresponding metal with oxidation state zero. More specifically, the doublets were located at about 368.3 and 374.3 eV (Figure 7b), which can be ascribed to the $3d_{5/2}$ and $3d_{3/2}$ levels of Ag^0, respectively; 335.3 and 340.6 eV (Figure 7c), attributed to the $3d_{5/2}$ and $3d_{3/2}$ levels of Pd^0, respectively; and 71.3 and 74.6 eV (Figure 7d), which can be associated with the $4f_{7/2}$ and $4f_{5/2}$ levels of Pt^0, respectively.[69] No components that could be associated with

DOI: 10.1021/acsami.5b00910
ACS Appl. Mater. Interfaces 2015, 7, 10293−10307

oxidized Ag, Pd, or Pt (e.g., Ag^+, Pd^{2+} or Pt^{4+}) were detected in the core level spectra, indicating that the NPs observed on the graphene sheets were generated in metallic form, as intended. The amount of metal on the graphene sheets was determined by inductively coupled plasma-mass spectrometry (ICP-MS), which yielded wt % loadings of metal to graphene of 40, 17, and 8 for graphene−metal NP hybrids decorated with Ag, Pd, and Pt, respectively.

To assess their catalytic activity, the graphene−metal NP hybrids were tested for two commonly studied model reactions, namely the reduction of *p*-nitrophenol (*p*-NP) to *p*-aminophenol (*p*-AP) and the reduction of *p*-nitroaniline (*p*-NA) to *p*-phenylenediamine (*p*-PDA) in the aqueous phase at room temperature, using $NaBH_4$ as a reductant. These reactions are also relevant from a practical point of view: for example, the reduction of *p*-NP to *p*-AP constitutes a key step in the synthesis of some analgesic and antipyretic drugs, such as paracetamol, whereas *p*-PDA obtained by reduction of *p*-NA is employed as a dye, as a rubber antioxidant, or in the preparation of aramid-based polymers (e.g., Kevlar).[70,71] Both reduction reactions are known to be thermodynamically favorable but are kinetically hindered by relatively high activation barriers, so that the mediating role of a catalyst becomes necessary for them to proceed at a convenient rate; in particular, noble metals such as Au, Ag, Pd, and Pt have been shown to be very efficient in this regard.[70] Furthermore, both reactions can be readily followed by UV−vis absorption spectroscopy. More specifically, under acidic or neutral conditions an aqueous *p*-NP solution exhibits a strong absorption band at ∼316 nm (Figure 8a, black trace). However, this peak red-shifts to about 400 nm at the basic pH generated in the presence of $NaBH_4$, which is due to deprotonation of *p*-NP to give the *p*-nitrophenolate anion (green trace). Upon reduction of the latter to the *p*-aminophenolate anion, a characteristic, relatively weak band appears at ∼295 nm, whereas no absorbance is detected at 400 nm (violet trace). Thus, the absorbance at 400 nm should be directly related to the concentration of *p*-nitrophenolate in the reaction medium, and consequently, monitoring such absorbance can be taken as a quantitative measure of the progress of this reduction reaction. Similarly, *p*-NA displays a well-defined absorption peak at ∼380 nm (Figure 8c, orange trace) that is not present in its reduced counterpart *p*-PDA (blue trace), so in this case absorbance at 380 nm can be used to monitor the reaction progress.

Figure 8b shows a typical kinetic curve for the catalyzed reduction of *p*-NP in the presence of the graphene−Pd NP hybrid, where the Pd NPs were prepared by the $NaBH_4$ reduction method. Similar curves were obtained with the other hybrids. For such a reaction, the kinetic profile could be reasonably well fitted to an exponential decay function for all the tested hybrids. Taking also into account that the concentration of the reducing agent ($NaBH_4$) should remain approximately constant throughout the reduction reaction as a result of its very high molar ratio with respect to *p*-NP (600:1; see Experimental Section), we can reasonably conclude that the reaction obeys a pseudo-first-order kinetic behavior with respect to the substrate, so that the following equation should apply:

$$\frac{d[p\text{-NP}]}{dt} = -k_{app}[p\text{-NP}] \quad (1)$$

where [*p*-NP] is the concentration of the substrate and k_{app} is the apparent reaction rate constant. Typical k_{app} values measured for the hybrids were on the order of 10^{-2} s^{-1} (e.g., see Figure 8b). By contrast, as exemplified in Figure 8d for the graphene−Ag NP hybrid, the reduction of *p*-NA frequently exhibited a linear decay in the recorded kinetic profiles, thereby suggesting a pseudozero-order reaction that obeys the equation:

$$\frac{d[p\text{-NA}]}{dt} = -k_{app} \quad (2)$$

with characteristic k_{app} values on the order of 10^{-3} mM s^{-1}. Catalyzed reactions with zero-order kinetics are usually associated with saturation of the catalytically active sites with adsorbed reactant molecules. As a plausible reason to explain why this would be the case in the reduction of *p*-NA but not for the similar reaction with *p*-NP, we note that access of the negatively charged *p*-nitrophenolate anions to the immediate vicinity of the graphene−metal NP hybrid in the aqueous medium would be hampered to some extent by the negative charge of the phosphate groups that decorate the FMNS-stabilized graphene sheets. This electrostatic effect would limit the number of *p*-nitrophenolate molecules than can adsorb on the metal NP surface to be reduced by the BH_4^- anion. On the other hand, the *p*-NA molecule is expected to be electrically neutral in the alkaline medium of the reaction, so that electrostatic barriers to adsorption will not be in place in this case, allowing for larger numbers of molecules to be adsorbed on, and possibly saturate, the NP surface. We also note that no conversion of *p*-NP to *p*-AP or of *p*-NA to *p*-PDA (i.e., no decay of the 400 or 380 nm peak intensity, respectively) was observed to occur in the presence of just FMNS or FMNS-stabilized graphene flakes, confirming the catalytic role of the metal NPs in the hybrids.

To compare the catalytic activity of the present hybrids with that of other noble metal-based catalysts reported in the literature for the same reactions, we calculated their turnover frequency (TOF), defined as the number of moles of substrate (i.e., *p*-NP or *p*-NA) converted per mole of metal catalyst used in the reaction (determined by ICP-MS) per unit time. Table 2 collects TOF values obtained for our hybrids as well as for a representative set of catalysts based on Au, Ag, Pd, and Pt nanostructures that have been previously studied for the reduction of either *p*-NP[72−88] or *p*-NA.[75,89−97] For the former reaction, the measured TOF values of our graphene−metal NP hybrids were typically in the range of a few to several min^{-1}, such activities being comparable to those of many of the best performing catalysts documented in recent years. The catalytic activity of the three hybrids was seen to be considerably higher in the case of *p*-NA reduction, with TOF values as high as 23 min^{-1} for the graphene−Pt NP hybrid. To the best of our knowledge, these are the highest activities that have been reported for such a reaction. These high catalytic activities can be attributed, at least in part, to the absence of any capping agents on the surface of the NPs anchored on the graphene flakes. When such substances are required to avoid agglomeration of the NPs in the liquid media, they can be easily adsorbed on the catallytically active sites of the surface, thus hampering access of the substrate molecule to such sites. In line with the previous reasoning, we ascribe the lower catalytic performance of our hybrids toward *p*-NP reduction relative to the *p*-NA case to electrostatic repulsion effects that hinder the

DOI: 10.1021/acsami.5b00910
ACS Appl. Mater. Interfaces 2015, 7, 10293−10307

Table 2. Comparison of Turnover Frequency (TOF) Values for Different Noble Metal-Based Catalysts in the Reduction of 4-NP and 4-NA with $NaBH_4$

catalyst	TOF (min^{-1})	ref
reduction of *p*-NP		
graphene-Ag NP hybrid	3.0	present work
graphene-Pd NP hybrid ($NaBH_4$)	3.4	present work
graphene-Pt NP hybrid	11	present work
5-nm-sized citrate-capped Au NPs	1.4	72
Au NPs deposited onto PMMA	1.5	73
Au NP/graphene hydrogel	0.19	74
hollow Ag nanospheres	0.16	75
Ag NP-chitosan composite	0.1	76
Ag NPs on carbon nanofibers	0.58	77
Ag NPs on alginate microspheres	1.9	78
Pt NPs	0.1	79
surfactant-capped Pt nanocubes	2.5	80
Pt NPs derived from wood nanomaterials	0.03−0.26	81
Pt NPs on Fe_2O_3/N-doped reduced graphene oxide hybrids	10.8	82
Pd NPs in graphene@carbon hollow spheres	4.56	83
Pd NPs on covalently funcionalized CNTs	18	84
Pd NPs supported onto CNT-graphene hydrogel	0.43	85
pentacle Au−Cu alloy nanocrystals	0.8−1.7	72
Pt−Au alloy NPs on ionic liquid-derived carbon	0.2	86
Au−Pd alloy nanodendrites	0.4	87
5-fold twinned $Ag_{0.6}Ni_{0.4}$ alloy NPs	0.22	88
reduction of *p*-NA		
graphene-Ag NP hybrid	9.2	present work
graphene-Pd NP hybrid ($NaBH_4$)	19	present work
graphene-Pt NP hybrid	23	present work
rhombic dodecahedral Au NPs	0.10	89
cubic Au NPs	0.08	89
octahedral Au NPs	0.02	89
Au NPs embedded in hydrogel matrix	0.49	90
Au nanowire networks	0.06−0.18	91
metal-oxide-supported Ag clusters	0.1	92
hollow Ag nanospheres	0.10	75
Fe_3O_4−3-aminopropyl-triethoxysilane/Pd composite	2.0	93
bimetallic Pt−Ni NPs	0.3	94
polyaniline/F_3O_4/PdNP hybrids	0.25	95
Fe_3O_4-supported Pd NPs	3	96
peptide stabilized Ag@Au core−shell NPs	0.7	97
5-fold twinned $Ag_{0.6}Ni_{0.4}$ alloy NPs	0.15	88

approaching of *p*-nitrophenolate anions to the NPs in the hybrids.

Finally, we tested the performance of the hybrids as electrocatalysts for the oxygen reduction reaction in view of its importance in the development of oxygen sensors and in fuel cell applications.[98] Compared to other techniques employed for oxygen determination (e. g., optical methods), electrochemical sensing has the advantages of simplicity, high sensitivity, low-cost, and the ability to analyze colored and/or turbid samples. Also, it only requires a low-power, compact instrumentation. The determination of dissolved oxygen levels is of great importance in many areas of industry, medicine, and the environment. To evaluate the electrocatalytic properties of graphene−metal NP hybrids toward oxygen electroreduction, linear sweep voltammograms (LSVs) in a 0.2 M NaOH solution in the presence and absence of oxygen were recorded with graphene−metal NP hybrid modified glassy carbon electrodes (GCEs). Figure 9 shows LSVs of oxygen reduction

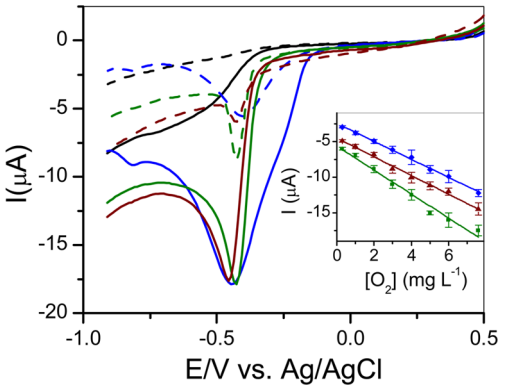

Figure 9. Linear-scan voltammograms of O_2 reduction at the graphene modified electrodes (total mass of deposited graphene: 0.6 μg) in O_2-saturated 0.2 M NaOH solution (solid lines) and N_2-saturated 0.2 M NaOH solution (dotted lines). The studied materials were graphene (black trace), graphene−Pt hybrid (blue trace) graphene−Pd NP hybrids prepared in EtOH (green trace), and graphene−Pd NP hybrids prepared with $NaBH_4$ (brown trace). Scan rate: 50 mVs^{-1}. The inset shows the corresponding O_2 calibration curves.

recorded with graphene-modified electrodes (0.6 μg) in O_2-saturated (solid lines) and N_2-saturated (dotted lines) 0.2 M NaOH solutions. The amount of graphene−metal NP hybrid was previously optimized by performing studies with different amounts of the hybrids in the presence of different concentrations of O_2 (see Supporting Information for details). In an O_2-saturated medium, a positive shift of the O_2 reduction wave potential was observed in the presence of graphene−Pt NP hybrid (blue trace) and graphene−Pd NP hybrid prepared with ethanol (green trace), and with $NaBH_4$ (brown trace) as a reductant, compared to that recorded with a graphene−FMNS electrode (black trace). No oxygen reduction peak was observed in N_2-saturated solution with the electrode modified with the FMNS-stabilized graphene sheets alone. However, cathodic peaks were recorded for all graphene−metal NP hybrids, which might be related to the presence of oxygen molecules strongly adsorbed on the NP surface. In addition to the potential shift, which is a clear indication of a catalytic process, a notable increase in the oxygen reduction current was registered in the presence of graphene−metal NP hybrids. The response of graphene−metal NP hybrid modified electrodes to O_2 concentration was also evaluated in 0.2 M NaOH solution by means of LSV. Similar calibration curves were obtained for all graphene−metal NP hybrids with a linear response range from 0.30 to 7.6 mg L^{-1} (see inset to Figure 9). Correlation coefficients of 0.997, 0.996, and 0.997 with limits of detection (LOD) of 0.25, 0.27, and 0.29 mg L^{-1} were calculated for graphene−Pt and graphene−Pd NP hybrids prepared with ethanol and $NaBH_4$, respectively. LODs were estimated as 3 times the standard deviation of the blank divided by the slope of the calibration curve. These results are similar to those obtained for other previously reported oxygen electrochemical sensors based on GCEs modified with poly(methylene blue)-doped silica nanocomposite,[99] cobalt tetrasulfonated phthalo-

DOI: 10.1021/acsami.5b00910
ACS Appl. Mater. Interfaces 2015, 7, 10293−10307

cyanine,[100] or with alternated layers of iron(II) tetrasulfonated phthalocyanine and iron(III) tetra-(*N*-methyl-pyridyl)-porphyrin,[101] which suggests that these graphene–metal NP hybrid materials could be used for the same purpose.

3. CONCLUSIONS

We have demonstrated the sodium salt of flavin mononucleotide (FMNS), an innocuous and widely available derivative of vitamin B_2, to be an exceptionally efficient dispersant for the preparation of few-layer graphene flakes in aqueous dispersion, obtained through ultrasonic exfoliation of graphite powder. Significantly, the graphene flakes could be colloidally stabilized in the aqueous phase by the assistance of rather small amounts of FMNS molecules (FMNS/graphene mass ratios of ~0.04), while achieving at the same time very high graphene concentrations (up to ~50 mg mL^{-1}). As a result of the low fraction of dispersant, graphene films prepared from these FMNS-stabilized dispersions exhibited improved conductivity values (~52 000 S m^{-1}), which should be useful for electrode applications. The presence of FMNS molecules adsorbed on the graphene surface was beneficial not only for the colloidal stabilization of the flakes but also for other purposes. As an example, we demonstrated the attachment and growth of nanoparticles of several noble metals (Ag, Pd, and Pt) on the sheets, and the resulting graphene–metal nanoparticle hybrids exhibited a high catalytic activity in the reduction of nitroarenes and a strong potential as electrocatalysts for oxygen sensing. The functionalization of the graphene sheets with phosphate groups that is inherently associated with the present FMNS-based approach might be useful as well in the hybridization of this two-dimensional carbon material with biomolecules (e.g., proteins or DNA) through the formation of phosphate diester linkages, which is of potential interest in biochemistry and/or biomedical applications.

4. EXPERIMENTAL SECTION

4.1. Preparation and Processing of FMNS-Stabilized Graphene Dispersions in Water. Unless otherwise stated, all the chemicals and starting materials used in this work were obtained from Sigma-Aldrich. In the preparation of aqueous FMNS-stabilized graphene dispersions, the effect of different experimental parameters was investigated, but a typical optimized procedure was as follows: natural graphite powder was added at a concentration of 30 mg mL^{-1} to an 1 mg mL^{-1} aqueous FMNS solution and sonicated for 5 h at a power of 20 W L^{-1} in an ultrasound bath cleaner (JP Selecta Ultrasons system, 40 kHz). After sonication, the obtained suspensions were centrifuged at 1500–2300 rpm for 20 min (Eppendorf 5424 microcentrifuge) to sediment unexfoliated graphite particles. The top ~75% of the resulting supernatant was a dispersion of FMNS-stabilized graphene sheets, which was collected for further use. To remove excess FMNS from the graphene dispersion, the exfoliated sheets were subjected to two cycles of sedimentation via centrifugation at 14 600 rpm for 20 min and resuspension in Milli-Q water through sonication for 1–2 min. Excess FMNS could be also removed from the dispersions through dialysis, using cellulose membranes with a molecular weight cutoff of 12 000 Da.

To assess the efficiency of FMNS as a stabilizer of graphene sheets in aqueous medium, the concentration of the different dispersions had to be determined. This was carried out by means of UV–vis absorption spectroscopy using a double-beam Heλios α spectrophotometer (Thermo Spectronic) on the basis of the Lambert–Beer law: $A/l = \alpha C$, where A is the measured absorbance, l is the optical path length, α is the extinction coefficient, and C is the graphene concentration. In line with previous reports,[19,22,24] A was determined at 660 nm, which is well within the wavelength range (>500 nm) where FMNS is completely transparent. α was estimated on the basis of graphene dispersions prepared in water–isopropanol mixtures in the absence of FMNS or any other stabilizer.[57] To this end, natural graphite powder was sonicated in a water–isopropanol mixture (volume ratio 65:35) for 5 h at an initial graphite concentration of 10 mg mL^{-1} and then centrifuged at 2300 rpm for 15 min. An aliquot of the resulting graphene dispersion (supernatant) was taken and serially diluted to obtain a series of dispersions with different concentrations, the absorbance of which was measured. The rest of the as-prepared dispersion, of a known volume, was completely sedimented by centrifugation (14 600 rpm, 30 min), dried in a vacuum oven (95 °C, 48 h), allowed to cool down in a desiccator, and finally weighed to calculate its original concentration. A calibration curve relating measured absorbance and graphene concentration could then be plotted, the slope of which yielded α. A value of α (660 nm) = 2440 mL mg^{-1} m^{-1} was determined. This figure is in good agreement with previous estimates for pristine graphene dispersed in several organic solvents[19] and in water–surfactant solutions.[25] Indication that the value for α derived here is also reasonably correct for determining the concentration of FMNS-stabilized graphene was attained from the observation that the weight of free-standing paper-like films prepared by vacuum filtration of aqueous dispersions with a low FMNS/graphene mass ratio was consistent with the graphene concentration in the dispersion estimated through the Lambert–Beer law.

4.2. Synthesis of Metal (Ag, Pt, Pd) NPs on FMNS-Stabilized Graphene Sheets. Graphene–metal NP hybrids were obtained as follows. In the case of Ag NPs, mixed aqueous solutions containing 0.1 mg mL^{-1} FMNS-stabilized graphene sheets, 0.5 mM $AgNO_3$, and 22.5 mM $NaBH_4$ as a reductant were prepared and left to react undisturbed at room temperature for 2 h. For the synthesis of Pt NPs, 9 mL of a 0.2 mg mL^{-1} aqueous FMNS-stabilized graphene dispersion was heated at 85 °C under magnetic stirring in a 20 mL test tube sealed with a septum, and then 1 mL of 1.1 mM aqueous K_2PtCl_6 solution was added. The resulting mixture was stirred for 2 h at this temperature and then cooled down to room temperature. To remove unreacted Pt salt, the dispersion was subjected to sedimentation via centrifugation at 14 600 rpm for 20 min and resuspension in Milli-Q water through sonication for 1–2 min. Subsequently, 20 μL of 1.5 M $NaBH_4$ was added and allowed to react for 45 min. As for the preparation of Pd NPs, two different protocols were used. In the first one, 9.7 mL of 0.1 mg mL^{-1} aqueous FMNS-stabilized graphene dispersion was heated at 70 °C under magnetic stirring in a 20 mL test tube sealed with a septum. Subsequently, 100 μL of 1.2 M $NaBH_4$ and 300 μL of 5.6 mM aqueous $PdCl_2$ solution were added to the dispersion, and the mixture was stirred at this temperature for 12 h. In the second protocol, a mixed solution containing 0.1 mg mL^{-1} FMNS-stabilized graphene sheets and 0.17 mM $PdCl_2$ in water–ethanol (volume ratio 1:1) was allowed to react at 60 °C for 90 min. Here, besides acting as a solvent, the ethanol molecules played the role of a reductant. In all cases, the resulting graphene–metal NP hybrids were purified by two cycles of sedimentation via centrifugation (14 600 rpm, 20 min) and resuspension in Milli-Q water.

4.3. Characterization Techniques. The samples were characterized by UV–vis absorption spectroscopy, ATR-FTIR spectroscopy, Raman spectroscopy, XPS, STEM, TEM, AFM, ICP-MS, voltammetric techniques, and measurement of electrical conductivity. ATR-FTIR spectra were recorded on a Nicolet 3700 spectrometer (Thermo Scientific) using diamond as the ATR crystal. Samples for this technique were free-standing paper-like graphene films obtained as explained below for the electrical conductivity measurements. Raman spectroscopy was accomplished with a Horiba Jobin-Yvon LabRam apparatus at a laser excitation wavelength of 532 nm. XPS measurements were carried out on a SPECS system under a pressure of 10^{-7} Pa with a nonmonochromatic Mg K_α X-ray source operated at 11.81 kV and 100 W. Specimens for both Raman and XPS analysis were prepared by drop-casting the aqueous dispersions onto a metallic sample-holder preheated at ~50–60 °C, which was then allowed to dry. STEM images were acquired on a Quanta FEG 650 system (FEI Company) operated at 30 kV, whereas TEM imaging was performed with a JEOL 2000 EX-II instrument operated at 160 kV. Specimens for both STEM and TEM were prepared by mixing equal volumes of the

DOI: 10.1021/acsami.5b00910
ACS Appl. Mater. Interfaces 2015, 7, 10293–10307

aqueous dispersion of the sample and ethanol. Then, 40 μL of the resulting suspension was drop-cast onto a copper grid (200 square mesh) covered with a carbon film (Electron Microscopy Sciences) and allowed to dry. AFM imaging was performed under ambient conditions with a Nanoscope IIIa Multimode apparatus (Veeco Instruments) in the tapping mode of operation. Rectangular silicon cantilevers with nominal spring constant and resonance frequency of about 40 N m^{-1} and 250−300 kHz were employed. Samples for AFM were prepared by drop-casting a small volume of diluted graphene dispersion (~0.05 mg mL^{-1}) onto a SiO_2 (300 nm)/Si substrate preheated at ~50−60 °C, which was subsequently allowed to dry. ICP-MS analyses of the graphene−metal NP hybrids were performed with a 7500ce (Agilent) instrument equipped with an octopole collision/reaction cell to destroy interfering ions. Prior to analysis, the hybrids were subjected to microwave-assisted acid digestion.

Voltammetric studies were carried out using an Autolab PGSTAT 12 (EcoChemie) potentiostat/galvanostat controlled by Autolab GPES software (version 4.9). All the measurements were accomplished using a three-electrode configuration cell, where a glassy carbon electrode (GCE; surface diameter ~3 mm, Metrohm) coated with the graphene sample under study deposited by drop-casting served as the working electrode. A Pt electrode and an Ag/AgCl electrode (Metrohm) were used as counter and reference electrodes, respectively. The GCE surface was renewed by polishing with 1.0 and 0.3 μm α-Al_2O_3 powders on a microcloth polishing pad (Sugelabor, S.A.), followed by washing in an ultrasonic bath for 2 min. For the measurement of electrical conductivity, free-standing paper-like graphene films were prepared by vacuum filtration of the corresponding aqueous dispersions through a silver membrane filter (47 mm in diameter and 0.2 μm of pore size, from Whatman). Then 12 ×12 mm^2 square pieces were cut from the films and their conductivity determined by the van der Pauw method using a homemade setup (Agilent 6614 DC potentiostat and Fluke 45 digital multimeter).

4.4. Catalytic and Electrocatalytic Activity of Graphene−Metal NP Hybrids. The catalytic activity of the graphene−metal NP hybrids was evaluated toward two model reactions involving nitroarenes: reduction of *p*-NP to *p*-AP and reduction of *p*-NA to *p*-PDA, in both cases at room temperature in aqueous medium and using $NaBH_4$ as the reducing agent. The reaction progress was monitored by means of UV−vis absorption spectroscopy. An excess amount of reductant was employed (molar ratio of $NaBH_4$ to either *p*-NP or *p*-NA, 600:1) to ensure that its concentration remained essentially constant throughout the reduction reaction. More specifically, mixed solutions containing 0.06 mM nitroarene, 36 mM $NaBH_4$, and 2−15 μg mL^{-1} FMNS-stabilized graphene sheets that incorporated the metal NPs at concentrations of 0.005−0.01 mM were freshly prepared and vigorously shaken for a few seconds before measuring their absorbance at a specific wavelength at 0.25 s time intervals. For *p*-NP, the absorbance was measured at 400 nm, which corresponds to the location of a characteristic peak of deprotonated *p*-NP (*p*-nitrophenolate anion) that forms in the basic medium generated in the presence of $NaBH_4$. This peak is not present in *p*-AP, so its intensity can be used to follow the conversion of *p*-NP to *p*-AP. Similarly, *p*-NA exhibits a strong peak at about 380 nm that is absent from *p*-PDA, so in this case the progress of the reduction reaction was traced by monitoring absorbance at the mentioned wavelength. To assess the electrocatalytic properties of the graphene−metal NP hybrids for the oxygen reduction reaction, linear sweep voltammograms (LSVs) were recorded onto GCEs coated with the hybrids deposited by drop-casting. The measurements were done in a 0.2 M NaOH medium in the presence of different concentrations of dissolved oxygen achieved by bubbling pure O_2 or N_2 into the solution. A commercial O_2 sensor (Seven Go pro/Inlab 605 dissolved oxygen meter Metler Toledo, Switzerland) was used to measure oxygen concentrations in the test solutions.

■ ASSOCIATED CONTENT

Supporting Information

Characterization of the starting graphite powder by elemental analysis and field-emission scanning electron microscopy (FE-SEM). Detailed characterization of the aqueous FMNS-stabilized graphene dispersion by TEM, AFM, ATR-FTIR, and Raman spectroscopy. Cyclic voltammograms of pure FMNS and pure riboflavin. Reusability studies of the graphene−metal NP hybrids as catalysts of the reduction of 4-NP to 4-NA with $NaBH_4$. Optimization of the amount of graphene−metal NP hybrid deposited on the GCE to perform the O_2 electroreduction studies. The Supporting Information is available free of charge on the ACS Publications website at DOI: 10.1021/acsami.5b00910.

■ AUTHOR INFORMATION

Corresponding Author

*Telephone: (+34) 985 11 90 90. Fax: (+34) 985 29 76 62. E-mail: silvia@incar.csic.es.

Notes

The authors declare no competing financial interest.

■ ACKNOWLEDGMENTS

Financial support from the Spanish Ministry of Economy and Competitiveness (MINECO) and the European Regional Development Fund (projects MAT2011-26399, and MAT2014-59592-R) is gratefully acknowledged. M.A.-V. is thankful for the receipt of a predoctoral contract (FPI) from MINECO.

■ REFERENCES

(1) Geim, A. K. Graphene: Status and Prospects. *Science* **2009**, *324*, 1530−1534.

(2) Novoselov, K. S.; Fal'ko, V. I.; Colombo, L.; Gellert, P. R.; Schwab, M. G.; Kim, K. A Roadmap for Graphene. *Nature* **2012**, *490*, 192−200.

(3) Ferrari, A. C.; Bonaccorso, F.; Falko, V.; Novoselov, K. S.; Roche, S.; Bøggild, P.; Borini, S.; Koppens, F.; Palermo, V.; Pugno, N.; Garrido, J. A.; Sordan, R.; Bianco, A.; Ballerini, L.; Prato, M.; Lidorikis, E.; Kivioja, J.; Marinelli, C.; Ryhänen, T.; Morpurgo, A.; Coleman, J. N.; Nicolosi, V.; Colombo, L.; Fert, A.; Garcia-Hernandez, M.; Bachtold, A.; Schneider, G. F.; Guinea, F.; Dekker, C.; Barbone, M.; Galiotis, C.; Grigorenko, A.; Konstantatos, G.; Kis, A.; Katsnelson, M.; Beenakker, C. W. J.; Vandersypen, L.; Loiseau, A.; Morandi, V.; Neumaier, D.; Treossi, E.; Pellegrini, V.; Polini, M.; Tredicucci, A.; Williams, G. M.; Hong, B. H.; Ahn, J. H.; Kim, J. M.; Zirath, H.; van Wees, B. J.; van der Zant, H.; Occhipinti, L.; Di Matteo, A.; Kinloch, I. A.; Seyller, T.; Quesnel, E.; Feng, X.; Teo, K.; Rupesinghe, N.; Hakonen, P.; Neil, S. R. T.; Tannock, Q.; Löfwander, T.; Kinaret, J. Science and Technology Roadmap for Graphene, Related Two-Dimensional Crystals, and Hybrid Systems. *Nanoscale* **2015**, *7*, 4598−4810.

(4) Bonaccorso, F.; Lombardo, A.; Hasan, T.; Sun, Z.; Colombo, L.; Ferrari, A. C. Production and Processing of Graphene and 2D Crystals. *Mater. Today* **2012**, *15*, 564−589.

(5) Li, X.; Cai, W.; An, J.; Kim, S.; Nah, J.; Yang, D.; Piner, R.; Velamakanni, A.; Jung, I.; Tutuc, E.; Banerjee, S. K.; Colombo, L.; Ruoff, R. S. Large-Area synthesis of High-Quality and Uniform Graphene Films on Copper Foils. *Science* **2009**, *324*, 1312−1314.

(6) Zhang, Y.; Zhang, L.; Zhou, C. Review of Chemical Vapor Deposition of Graphene and Related applications. *Acc. Chem. Res.* **2013**, *46*, 2329−2339.

(7) Cai, M.; Thorpe, D.; Adamson, D. H.; Schniepp, H. C. Methods of Graphite Exfoliation. *J. Mater. Chem.* **2012**, *22*, 24992−25002.

DOI: 10.1021/acsami.5b00910
ACS Appl. Mater. Interfaces 2015, 7, 10293−10307

(8) Zhong, Y. L.; Tian, Z.; Simon, G. P.; Li, D. Scalable Production of Graphene via Wet Chemistry: Progress and Challenges. *Mater. Today* **2015**, *18*, 73−78.
(9) Park, S.; Ruoff, R. S. Chemical Methods for the Production of Graphenes. *Nat. Nanotechnol.* **2009**, *4*, 217−224.
(10) Dreyer, D. R.; Park, S.; Bielawski, C. W.; Ruoff, R. S. The Chemistry of Graphene Oxide. *Chem. Soc. Rev.* **2010**, *39*, 228−240.
(11) Compton, O. C.; Nguyen, S. T. Graphene Oxide, Highly Reduced Graphene Oxide, and Graphene: Versatile Building Blocks for Carbon-Based Materials. *Small* **2010**, *6*, 711−723.
(12) Loh, K. P.; Bao, Q.; Eda, G.; Chhowalla, M. Graphene Oxide as a Chemically Tunable Platform for Optical Applications. *Nat. Chem.* **2010**, *2*, 1015−1024.
(13) Morales-Narváez, E.; Merkoçi, A. Graphene Oxide as an Optical Biosensing Platform. *Adv. Mater.* **2012**, *24*, 3298−3308.
(14) Pei, S.; Cheng, H.-M. The Reduction of Graphene Oxide. *Carbon* **2012**, *50*, 3210−3228.
(15) Mao, S.; Pu, H.; Chen, J. Graphene Oxide and its Reduction: Modeling and Experimental Progress. *RSC Adv.* **2012**, *2*, 2643−2662.
(16) Coleman, J. N. Liquid Exfoliation of Defect-Free Graphene. *Acc. Chem. Res.* **2013**, *46*, 14−22.
(17) Du, W.; Jiang, X.; Zhu, L. J. From Graphite to Graphene: Direct Liquid-Phase Exfoliation of Graphite to Produce Single- and Few-Layered Pristine Graphene. *J. Mater. Chem. A* **2013**, *1*, 10592−10606.
(18) Ciesielski, A.; Samorì, P. Graphene via Sonication Assisted Liquid-Phase Exfoliation. *Chem. Soc. Rev.* **2014**, *43*, 381−398.
(19) Hernandez, Y.; Nicolosi, V.; Lotya, M.; Blighe, F. M.; Sun, Z.; De, S.; McGovern, I. T.; Holland, B.; Byrne, M.; Guńko, Y. K.; Boland, J. J.; Niraj, P.; Duesberg, G.; Krishnamurthy, S.; Goodhue, R.; Hutchison, J.; Scardaci, V.; Ferrari, A. C.; Coleman, J. N. High-yield Production of Graphene by Liquid-Phase Exfoliation of Graphite. *Nat. Nanotechnol.* **2008**, *3*, 563−568.
(20) Hernandez, Y.; Lotya, M.; Rickard, D.; Bergin, S. D.; Coleman, J. N. Measurement of Multicomponent Solubility Parameters for Graphene Facilitates Solvent Discovery. *Langmuir* **2010**, *26*, 3208−3213.
(21) Ricardo, K. B.; Sendecki, A.; Liu, H. Surfactant-Free Exfoliation of Graphite in Aqueous Solutions. *Chem. Commun.* **2014**, *50*, 2751−2754.
(22) Lotya, M.; Hernandez, Y.; King, P. J.; Smith, R. J.; Nicolosi, V.; Karlsson, L. S.; Blighe, F. M.; De, S.; Wang, Z.; McGovern, I. T.; Duesberg, G. S.; Coleman, J. N. Liquid Phase Production of Graphene by Exfoliation of Graphite in Surfactant/Water Solutions. *J. Am. Chem. Soc.* **2009**, *131*, 3611−3620.
(23) De, S.; King, P. J.; Lotya, M.; O'Neill, A.; Doherty, E. M.; Hernandez, Y.; Duesberg, G. S.; Coleman, J. N. Flexible, Transparent, Conducting Films of Randomly Stacked Graphene from Surfactant-Stabilized, Oxide-Free Graphene Dispersions. *Small* **2010**, *6*, 458−464.
(24) Guardia, L.; Fernández-Merino, M. J.; Paredes, J. I.; Solís-Fernández, P.; Villar-Rodil, S.; Martínez-Alonso, A.; Tascón, J. M. D. High-Throughput Production of Pristine Graphene in an Aqueous Dispersion Assisted by Non-Ionic Surfactants. *Carbon* **2011**, *49*, 1653−1662.
(25) Sun, Z.; Masa, J.; Liu, Z.; Schuhmann, W.; Muhler, M. Highly Concentrated Aqueous Dispersions of Graphene Exfoliated by Sodium Taurodeoxycholate: Dispersion Behavior and Potential Application as a Catalyst Support for the Oxygen-Reduction Reaction. *Chem.—Eur. J.* **2012**, *18*, 6972−6978.
(26) Buzaglo, M.; Shtein, M.; Kober, S.; Lovrinčić, R.; Vilan, A.; Regev, O. Critical Parameters in Exfoliating Graphite into Graphene. *Phys. Chem. Chem. Phys.* **2013**, *15*, 4428−4435.
(27) Wang, Z.; Liu, J.; Wang, W.; Chen, H.; Liu, Z.; Yu, Q.; Zeng, H.; Sun, L. Aqueous Phase Preparation of Graphene with Low Defect Density and Adjustable Layers. *Chem. Commun.* **2013**, *49*, 10835−10837.
(28) Bourlinos, A. B.; Georgakilas, V.; Zboril, R.; Steriotis, T. A.; Stubos, A. K.; Trapalis, C. Aqueous-Phase Exfoliation of Graphite in the Presence of Polyvinylpyrrolidone for the Production of Water-Soluble Graphenes. *Solid State Commun.* **2009**, *149*, 2172−2176.
(29) Seo, J.-W. T.; Green, A. A.; Antaris, A. L.; Hersam, M. C. High-Concentration Aqueous Dispersions of Graphene using Nonionic, Biocompatible Block Copolymers. *J. Phys. Chem. Lett.* **2011**, *2*, 1004−1008.
(30) Salavagione, H. J.; Ellis, G.; Segura, J. L.; Gómez, R.; Morales, G. M.; Martínez, G. Flexible Film Materials from Conjugated Dye-Modified Polymer Surfactant-Induced Aqueous Graphene Dispersions. *J. Mater. Chem.* **2011**, *21*, 16129−16135.
(31) Notley, S. M. Highly Concentrated Suspensions of Graphene through Ultrasonic Exfoliation with Continuous Surfactant Addition. *Langmuir* **2012**, *28*, 14110−14113.
(32) Mao, M.; Chen, S.; He, P.; Zhang, H.; Liu, H. Facile and Economical Mass Production of Graphene Dispersions and Flakes. *J. Mater. Chem. A* **2014**, *2*, 4132−4135.
(33) Sun, Z.; Vivekananthan, J.; Guschin, D. A.; Huang, X.; Kuznetsov, V.; Ebbinghaus, P.; Sarfraz, A.; Muhler, M.; Schuhmann, W. High-Concentration Graphene Dispersions with Minimal Stabilizer: A Scaffold for Enzyme Immobilization for Glucose Oxidation. *Chem.—Eur. J.* **2014**, *20*, 5752−5761.
(34) Englert, J. M.; Röhrl, J.; Schmidt, C. D.; Graupner, R.; Hundhausen, M.; Hauke, F.; Hirsch, A. Soluble Graphene: Generation of Aqueous Graphene Solutions Aided by a Perylenebisimide-Based Bolaamphiphile. *Adv. Mater.* **2009**, *21*, 4265−4269.
(35) An, X.; Simmons, T.; Shah, R.; Wolfe, C.; Lewis, K. M.; Washington, M.; Nayak, S. K.; Talapatra, S.; Kar, S. Stable Aqueous Dispersions of Noncovalently Functionalized Graphene from Graphite and their Multifunctional High-Performance Applications. *Nano Lett.* **2010**, *10*, 4295−4301.
(36) Parviz, D.; Das, S.; Ahmend, H. S. T.; Irin, F.; Bhattacharia, S.; Green, M. J. Dispersions of Non-Covalently Functionalized Graphene with Minimal Stabilizer. *ACS Nano* **2012**, *6*, 8857−8867.
(37) Sampath, S.; Basuray, A. N.; Hartlieb, K. J.; Aytun, T.; Stupp, S. I.; Stoddart, J. F. Direct Exfoliation of Graphite to Graphene in Aqueous Media with Diazaperopyrenium Dications. *Adv. Mater.* **2013**, *25*, 2740−2745.
(38) Schlierf, A.; Yang, H.; Gebremedhn, E.; Treossi, E.; Ortolani, L.; Chen, L.; Minoia, A.; Morandi, V.; Samorì, P.; Casiraghi, C.; Beljonne, D.; Palermo, V. Nanoscale Insight into the Exfoliation Mechanism of Graphene with Organic Dyes: Effect of Charge, Dipole and Molecular Structure. *Nanoscale* **2013**, *5*, 4205−4216.
(39) Zhang, L.; Zhang, Z.; He, C.; Dai, L.; Liu, J.; Wang, L. Rationally Designed Surfactants for Few-Layered Graphene Exfoliation: Ionic Groups Attached to Electron-Deficient π-Conjugated Unit through Alkyl Spacers. *ACS Nano* **2014**, *8*, 6663−6670.
(40) Laaksonen, P.; Kainlauri, M.; Laaksonen, T.; Shchepetov, A.; Jiang, H.; Ahopelto, J.; Linder, M. B. Interfacial Engineering by Proteins: Exfoliation and Functionalization of Graphene by Hydrophobins. *Angew. Chem., Int. Ed.* **2010**, *49*, 4946−4949.
(41) Sharifi, F.; Bauld, R.; Ahmed, M. S.; Fanchini, G. Transparent and Conducting Graphene-RNA-Based Nanocomposites. *Small* **2012**, *8*, 699−706.
(42) Zhang, F.; Chen, X.; Boulos, R. A.; Yasin, F. M.; Lu, H.; Raston, C.; Zhang, H. Pyrene-Conjugated Hyaluronan Facilitated Exfoliation and Stabilisation of Low Dimensional Nanomaterials in Water. *Chem. Commun.* **2013**, *49*, 4845−4847.
(43) Chabot, V.; Kim, B.; Sloper, B.; Tzoganakis, C.; Yu, A. High Yield Production and Purification of Few Layer Graphene by Gum Arabic Assisted Physical Sonication. *Sci. Rep.* **2013**, *3*, 1378−1−1378−7.
(44) Qu, K.; Wu, L.; Ren, J.; Qu, X. Enzyme-Directed pH-Responsive Exfoliation and Dispersion of Graphene and its Decoration by Gold Nanoparticles for Use as a Hybrid Catalyst. *Nano Res.* **2013**, *6*, 693−702.
(45) Ihiawakrim, D.; Ersen, O.; Melin, F.; Hellwig, P.; Janowska, I.; Begin, D.; Baaziz, W.; Begin-Colin, S.; Pham-Huu, C.; Baati, R. A Single-Stage Functionalization and Exfoliation Method for the Production of Graphene in Water: Stepwise Construction of 2D-Nanostructured Composites with Iron Oxide Nanoparticles. *Nanoscale* **2013**, *5*, 9073−9080.

DOI: 10.1021/acsami.5b00910
ACS Appl. Mater. Interfaces 2015, 7, 10293−10307

(46) Holzer, W.; Shirdel, J.; Zirak, P.; Penzkofer, A.; Hegemann, P.; Deutzmann, R.; Hochmuth, E. Photo-Induced Degradation of Some Flavins in Aqueous Solution. *Chem. Phys.* **2005**, *308*, 69−78.
(47) Yoon, W.; Lee, Y.; Jang, H.; Jang, M.; Kim, J. S.; Lee, H. S.; Im, S.; Boo, D. W.; Park, J.; Ju, S.-Y. Graphene Nanoribbons Formed by a Sonochemical Graphene Unzipping Using Flavin Mononucleotide as a Template. *Carbon* **2015**, *81*, 629−638.
(48) Ju, S.-Y.; Doll, J.; Sharma, I.; Papadimitrakopoulos, F. Selection of Carbon Nanotubes with Specific Chiralities Using Helical Assemblies of Flavin Mononucleotide. *Nat. Nanotechnol.* **2008**, *3*, 356−362.
(49) Ju, S.-Y.; Abanulo, D. C.; Badalucco, C. A.; Gascón, J. A.; Papadimitrakopoulos, F. Handedness Enantioselection of Carbon Nanotubes Using Helical Assemblies of Flavin Mononucleotide. *J. Am. Chem. Soc.* **2012**, *134*, 13196−13199.
(50) Insińska-Rak, M.; Sikorski, M. Riboflavin Interactions with Oxygen—A Survey from the Photochemical Perspective. *Chem.—Eur. J.* **2014**, *20*, 15280−15291.
(51) Kammler, L.; Van Gastel, M. Electronic Structure of the Lowest Triplet State of Flavin Mononucleotide. *J. Phys. Chem. A* **2012**, *116*, 10090−10098.
(52) Li, D.; Müller, M. B.; Gilje, S.; Kaner, R. B.; Wallace, G. G. Processable Aqueous Dispersions of Graphene Nanosheets. *Nat. Nanotechnol.* **2008**, *3*, 101−105.
(53) Fernández-Merino, M. J.; Villar-Rodil, S.; Paredes, J. I.; Solís-Fernández, P.; Guardia, L.; García, R.; Martínez-Alonso, A.; Tascón, J. M. D. Identifying Efficient Natural Bioreductants for the Preparation of Graphene and Graphene-Metal Nanoparticle Hybrids with Enhanced Catalytic Activity from Graphite Oxide. *Carbon* **2013**, *63*, 30−44.
(54) Guardia, L.; Paredes, J. I.; Rozada, R.; Villar-Rodil, S.; Martínez-Alonso, A.; Tascón, J. M. D. Production of Aqueous Dispersions of Inorganic Graphene Analogues by Exfoliation and Stabilization with Non-Ionic Surfactants. *RSC Adv.* **2014**, *4*, 14115−14127.
(55) Cravotto, G.; Cintas, P. Sonication-Assisted Fabrication and Post-Synthetic Modifications of Graphene-Like Materials. *Chem.—Eur. J.* **2010**, *16*, 5246−5259.
(56) Łukasiewicz, J.; Grajek, H.; Frąckowiak, D. The Influence of Flavo Nucleotide (FMN) Dimerization on the Efficiency of the FMN Triplet States Generation. *Dyes Pigment.* **2007**, *73*, 377−382.
(57) Halim, U.; Zheng, C. R.; Chen, Y.; Lin, Z.; Jiang, S.; Cheng, R.; Huang, Y.; Duan, X. A rational Design of Cosolvent Exfoliation of Layered Materials by Directly Probing Liquid−Solid Interaction. *Nat. Commun.* **2013**, *4*, 2213−1−2213−7.
(58) Paton, K. R.; Varrla, E.; Backes, C.; Smith, R. J.; Khan, U.; O'Neil, A.; Boland, C.; Lotya, M.; Istrate, O. M.; King, P.; Higgins, T.; Barwich, S.; May, P.; Puczkarski, P.; Ahmed, I.; Moebius, M.; Pettersson, H.; Long, E.; Coelho, J.; O'Brien, S. E.; McGuire, E. K.; Mendoza Sanchez, B.; Duesberg, G. S.; McEvoy, N.; Pennycook, T. J.; Downing, C.; Crossley, A.; Nicolosi, V.; Coleman, J. N. Scalable Production of Large Quantities of Defect-Free Few-Layer Graphene by Shear Exfoliation in Liquids. *Nat. Mater.* **2014**, *13*, 624−630.
(59) Khan, U.; O'Neill, A.; Lotya, M.; De, S.; Coleman, J. N. High-Concentration Solvent Exfoliation of Graphene. *Small* **2010**, *6*, 864−871.
(60) Hamilton, C. E.; Lomeda, J. R.; Sun, Z.; Tour, J. M.; Barron, A. R. High-Yield Organic Dispersions of Graphene. *Nano Lett.* **2009**, *9*, 3460−3462.
(61) Parvez, P.; Wu, Z.-S.; Li, R.; Liu, X.; Graf, R.; Feng, X.; Müllen, K. Exfoliation of Graphite into Graphene in Aqueous Solutions of Inorganic Salts. *J. Am. Chem. Soc.* **2014**, *136*, 6083−6091.
(62) Park, K. H.; Kim, B. H.; Song, S. H.; Kwon, J.; Kong, B. S.; Kang, K.; Jeon, S. Exfoliation of Non-Oxidized Graphene Flakes for Scalable Conductive Film. *Nano Lett.* **2012**, *12*, 2871−2876.
(63) Behabtu, N.; Lomeda, J. R.; Green, M. J.; Higginbotham, A. L.; Sinitskii, A.; Kosynkin, D. V.; Tsentalovich, D.; Parra-Vasquez, A. N. G.; Schmidt, J.; Kesselman, E.; Cohen, Y.; Talmon, Y.; Tour, J. M.; Pasquali, M. Spontaneous High-Concentration Dispersions and Liquid Crystals of Graphene. *Nat. Nanotechnol.* **2010**, *5*, 406−411.
(64) Berchmans, S.; Vijayavalli, R. Surface Modification of Glassy-Carbon by Riboflavin. *Langmuir* **1996**, *11*, 286−290.
(65) Machado, B. F.; Serp, P. Graphene-Based Materials for Catalysis. *Catal. Sci. Technol.* **2012**, *2*, 54−75.
(66) Xiang, Q.; Yu, J.; Jaroniec, M. Graphene-Based Semiconductor Photocatalysts. *Chem. Soc. Rev.* **2012**, *41*, 782−796.
(67) Xia, B. Y.; Yan, Y.; Wang, X.; Lou, X. W. Recent Progress on Graphene-Based Hybrid Electrocatalysts. *Mater. Horiz.* **2014**, *1*, 379−399.
(68) Sun, Y.; Xia, Y. Gold and silver nanoparticles: A Class of Chromophores with Colors Tunable in the Range from 400 to 750 nm. *Analyst* **2003**, *128*, 686−691.
(69) Crist, B. V. *Handbook of Monochromatic XPS Spectra*; XPS International LLC: Mountain View, CA, 2004; Vol. *1*. The Elements and Native Oxides.
(70) Hervés, P.; Pérez-Lorenzo, M.; Liz-Marzán, L. M.; Dzubiella, J.; Lu, Y.; Ballauff, M. Catalysis by Metallic Nanoparticles in Aqueous Solution: Model Reactions. *Chem. Soc. Rev.* **2012**, *41*, 5577−5587.
(71) Wu, W.; Liu, G.; Liang, S.; Chen, Y.; Shen, L.; Zheng, H.; Yuan, R.; Hou, Y.; Wu, L. Efficient Visible-Light-Induced Photocatalytic Reduction of 4-Nitroaniline to *p*-Phenylenediamine over Nanocrystalline $PbBi_2Nb_2O_9$. *J. Catal.* **2012**, *290*, 13−17.
(72) He, R.; Wang, Y.-C.; Wang, X.; Wang, Z.; Liu, G.; Zhou, W.; Wen, L.; Li, Q.; Wang, X.; Chen, X.; Zeng, J.; Hou, J. G. Facile Synthesis of Pentacle Gold-Copper Alloy Nanocrystals and their Plasmonic and Catalytic Properties. *Nat. Commun.* **2014**, *5*, 4327−1−4327−10.
(73) Kuroda, K.; Ishida, T.; Haruta, M. Reduction of 4-Nitrophenol to 4-Aminophenol over Au Nanoparticles Deposited on PMMA. *J. Mol. Catal. A: Chem.* **2009**, *298*, 7−11.
(74) Li, J.; Liu, C.-Y.; Liu, Y. Au/Graphene Hydrogel: Synthesis, Characterization and its Use for Catalytic Reduction of 4-Nitrophenol. *J. Mater. Chem.* **2012**, *22*, 8426−8430.
(75) Vadakkekara, R.; Chakraborty, M.; Parikh, P. A. Reduction of Aromatic Nitro Compounds on Colloidal Hollow Silver Nanospheres. *Colloids Surf., A* **2012**, *399*, 11−17.
(76) Murugadoss, A.; Chattopadhyay, A. A 'Green' Chitosan−Silver Nanoparticle Composite as a Heterogeneous as well as Micro-Heterogeneous Catalyst. *Nanotechnology* **2008**, *19*, 015603−1−015603−9.
(77) Zhang, P.; Shao, C.; Zhang, Z.; Zhang, M.; Mu, J.; Guo, Z.; Liu, Y. In Situ Assembly of Well-Dispersed Ag Nanoparticles (AgNPs) on Electrospun Carbon Nanofibers (CNFs) for Catalytic Reduction of 4-Nitrophenol. *Nanoscale* **2011**, *3*, 3357−3363.
(78) You, J.; Zhao, C.; Cao, J.; Zhou, J.; Zhang, L. Fabrication of High-Density Silver Nanoparticles on the Surface of Alginate Microspheres for Application in Catalytic Reaction. *J. Mater. Chem. A* **2014**, *2*, 8491−8499.
(79) Xu, Y.; Wang, L.; Jiang, W.; Wang, H.; Yao, J.; Guo, Q.; Yuan, L.; Chen, H. Silicon Nanowire Arrays − A New Catalyst for the Reduction of Nitrobenzene Derivatives. *ChemCatChem.* **2013**, *5*, 3788−3793.
(80) Kim, C.; Lee, H. Change in the Catalytic Activity of Pt Nanocubes in the Presence of Different Surface-Capping Agents. *Catal. Commun.* **2009**, *10*, 1305−1309.
(81) Lin, X.; Wu, M.; Wu, D.; Kuga, S.; Endo, T.; Huang, Y. Platinum Nanoparticles Using Wood Nanomaterials: Eco-Friendly Synthesis, Shape Control and Catalytic Activity for *p*-Nitropheneol Reduction. *Green Chem.* **2011**, *13*, 283−287.
(82) Dai, Y.; Chai, Y.; Sun, Y.; Fu, W.; Wang, X.; Gu, Q.; Zeng, T. H.; Sun, Y. New Versatile Pt Supports Composed of Graphene Sheets Decorated by Fe_2O_3 Nanorods and N-Dopants with High Activity Based on Improved Metal/Support Interactions. *J. Mater. Chem. A* **2015**, *3*, 125−130.
(83) Zhang, Z.; Xiao, F.; Xi, J.; Sun, T.; Xiao, S.; Wang, H.; Wang, S.; Liu, Y. Encapsulating Pd Nanoparticles in Double-Shelled Graphene@Carbon Hollow Spheres for Excellent Chemical Catalytic Property. *Sci. Rep.* **2014**, *4*, 4053−1−4053−5.

DOI: 10.1021/acsami.5b00910
ACS Appl. Mater. Interfaces 2015, 7, 10293−10307

(84) Gu, X.; Qi, W.; Xu, X.; Sun, Z.; Zhang, L.; Liu, W.; Pan, X.; Su, D. Covalently Functionalized Carbon Nanotube Supported Pd Nanoparticles for Catalytic Reduction of 4-Nitrophenol. *Nanoscale* **2014**, *6*, 6609−6616.
(85) Zhang, Z.; Sun, T.; Chen, C.; Xiao, F.; Gong, Z.; Wang, S. Bifunctional Nanocatalyst Based on Three-Dimensional Carbon Nanotube−Graphene Hydrogel Supported Pd Nanoparticles: One-Pot Synthesis and its Catalytic Properties. *ACS Appl. Mater. Interfaces* **2014**, *6*, 21035−21040.
(86) Peng, Y.; Wu, X.; Qiu, L.; Liu, C.; Wang, S.; Yan, F. Synthesis of Carbon−PtAu Nanoparticle Hybrids Originating from Triethoxysilane-Derivatized Ionic Liquids for Methanol Electrooxidation and the Catalytic Reduction of 4-Nitrophenol. *J. Mater. Chem. A* **2013**, *1*, 9257−9263.
(87) Shi, L.; Wang, A.; Zhang, T.; Zhang, B.; Su, D.; Li, H.; Song, Y. One-Step Synthesis of Au−Pd Alloy Nanodendrites and their Catalytic Activity. *J. Phys. Chem. C* **2013**, *117*, 12526−12536.
(88) Kumar, M.; Deka, S. Multiply Twinned AgNi Alloy Nanoparticles as Highly Active Catalyst for Multiple Reduction and Degradation Reactions. *ACS Appl. Mater. Interfaces* **2014**, *6*, 16071−16081.
(89) Chiu, C.-Y.; Chung, P.-J.; Lao, K.-U.; Liao, C.-W.; Huang, M. H. Facet-Dependent Catalytic Activity of Gold Nanocubes, Octahedra, and Rhombic Dodecahedra toward 4-Nitroaniline Reduction. *J. Phys. Chem. C* **2012**, *116*, 23757−23763.
(90) Ramtenki, V.; Anumon, V. D.; Badiger, M. V.; Prasad, B. L. V. Gold nanoparticle embedded hydrogel matrices as catalysts: Better Dispersibility of Nanoparticles in the Gel Matrix upon Addition of N-Bromosuccinimide Leading to Increased Catalytic Efficiency. *Colloids Surf., A* **2012**, *414*, 296−301.
(91) Chirea, M.; Freitas, A.; Vasile, B. S.; Ghitulica, C.; Pereira, C. M.; Silva, F. Gold Nanowire Networks: Synthesis, Characterization, and Catalytic Activity. *Langmuir* **2011**, *27*, 3906−3913.
(92) Leelavathi, A.; Rao, T. U. B.; Pradeep, T. Supported Quantum Clusters of Silver as Enhanced Catalysts for Reduction. *Nanoscale Res. Lett.* **2011**, *6*, 123−1−123−9.
(93) Karaoglu, E.; Summak, M. M.; Baykal, A.; Sözeri, H.; Toprak, M. S. Synthesis and Characterization of Catalytically Activity Fe_3O_4-3-Aminopropyltriethoxysilane/Pd Nanocomposite. *J. Inorg. Organomet. Polym.* **2013**, *23*, 409−417.
(94) Ghosh, S. K.; Mandal, M.; Kundu, S.; Nath, S.; Pal, T. Bimetallic Pt−Ni Nanoparticles Can Catalyze Reduction of Aromatic Nitro Compounds by Sodium Borohydride in Aqueous Solution. *Appl. Catal., A* **2004**, *268*, 61−66.
(95) Kong, L.; Lu, X.; Jin, E.; Jiang, S.; Bian, X.; Zhang, W.; Wang, C. Constructing Magnetic Polyaniline/metal Hybrid Nanostructures Using Polyaniline/Fe_3O_4 Composite Hollow Spheres as Supports. *J. Solid State Chem.* **2009**, *182*, 2081−2087.
(96) Baykal, A.; Karaoglu, E.; Sözeri, H.; Uysal, E.; Toprak, M. S. Synthesis and Characterization of High Catalytic Activity Magnetic Fe_3O_4 Supported Pd Nanocatalyst. *J. Supercond. Nov. Magn.* **2013**, *26*, 165−171.
(97) Biswas, A.; Roy, S.; Banerjee, A. Peptide stabilized Ag@Au Core-Shell Nanoparticles: Synthesis, Variation of Shell Thickness, and Catalysis. *Z. Anorg. Allg. Chem.* **2014**, *640*, 1205−1211.
(98) Liu, M.; Zhang, R.; Chen, W. Graphene-supported Nanoelectrocatalysts for Fuel Cells: Synthesis, Properties, and Applications. *Chem. Rev.* **2014**, *114*, 5117−5160.
(99) Xiao, X.; Zhou, B.; Tan, L.; Tang, H.; Zhang, Y.; Xie, Q.; Yao, S. Poly (Methylene Blue) Silica Doped Nanocomposites with Cross-linked Cage Structure: Electropolymerization, Characterization, and Catalytic Activity for Reduction of Dissolved Oxygen. *Electrochim. Acta* **2011**, *56*, 10055−10063.
(100) Luz, R. C. S.; Damos, F. S.; Tanakab, A. A.; Kubota, L. T. Dissolved Oxygen Sensor Based on Cobalt Tetrasulphonated Phthalocyanine Immobilized in Poly-L-Lysine Film onto Glassy Carbon Electrode. *Sens. Actuators, B* **2006**, *114*, 1019−1027.
(101) Duarte, J. C.; Luz, R. C. S.; Damos, F. S.; Tanakab, A. A.; Kubota, L. T. A Highly Sensitive Amperometric Sensor for Oxygen Based on Iron(II) Tetrasulfonated Phthalocyanine and Iron(III) Tetra-(N-Methyl-Pyridyl)-Porphyrin Multilayers. *Anal. Chim. Acta* **2008**, *612*, 29−36.

DOI: 10.1021/acsami.5b00910
ACS Appl. Mater. Interfaces 2015, 7, 10293−10307